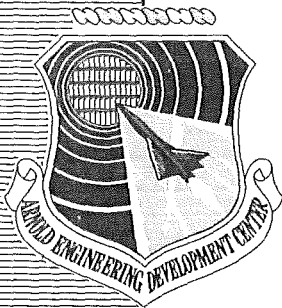


AEDC-TDR-63-206

ARCHIVE COPY
DO NOT LOAN

Cy. 1



PROBLEMS IN COMPUTING RADIATION CONTROL FUNCTIONS FOR MARK I

By

Cord H. Link, Jr.

Scientific Computing Services
Office of the Director of Engineering
ARO, Inc.

TECHNICAL DOCUMENTARY REPORT NO. AEDC-TDR-63-206

February 1964

(Prepared under Contract No. AF 40(600)-1000 by ARO, Inc.,
contract operator of AEDC, Arnold Air Force Station, Tenn.)

AEDC TECHNICAL LIBRARY



ARNOLD ENGINEERING DEVELOPMENT CENTER
AIR FORCE SYSTEMS COMMAND
UNITED STATES AIR FORCE

PROPERTY OF U. S. AIR FORCE
AEDC LIBRARY
AF 40(600)1000

NOTICES

Qualified requesters may obtain copies of this report from DDC, Cameron Station, Alexandria, Va. Orders will be expedited if placed through the librarian or other staff member designated to request and receive documents from DDC.

When Government drawings, specifications or other data are used for any purpose other than in connection with a definitely related Government procurement operation, the United States Government thereby incurs no responsibility nor any obligation whatsoever; and the fact that the Government may have formulated, furnished, or in any way supplied the said drawings, specifications, or other data, is not to be regarded by implication or otherwise as in any manner licensing the holder or any other person or corporation, or conveying any rights or permission to manufacture, use, or sell any patented invention that may in any way be related thereto.

Errata AEDC-TDR-63-206, February 1964 [†]

Please note the following corrections:

Page 25. Fig. 15. The arrows of the center figure should be reversed, and the phrase (Advance of Line of Nodes) should be deleted.

Page 28. Footnote. Change Move strictly to *More strictly.

Page 44. First equation. $(d, \beta, \theta_S, \gamma)$ should be changed to $(\alpha, \beta, \theta_S, \gamma)$.

Page 50. 3(a). Add 2π as in 1(a).
Second equation from bottom of page. Add $\} / \sin \gamma$ to the end of line.
Last equation on page. $a_e I_S$ should be changed to $a_e I_S$ and $+\sin^2 \gamma$ should be inserted after $\sin^3 \gamma$.

Page 51. Line 4. should be changed to $\cos^2 \beta \sin \beta \sin \psi \cos \alpha d\alpha d\beta$.

Page 52. The line 7. should be line 9. and line 8. should be line 10.
Line (7, 8) (a) should be line (9, 10) (a).

On the thirteenth line, the equation should be changed to

$$\frac{1}{\sin \gamma} \left[\frac{3}{4} \gamma - \sin \gamma \cos \gamma + \frac{1}{4} (\sin \gamma \cos^3 \gamma - \cos \gamma \sin^3 \gamma) \right]$$

On the fifteenth line, the equation should be changed to

$$\frac{I_2}{\Delta A_2} = \frac{a_e I_S}{8} \left[\sin^3 \gamma + \frac{2}{\pi \sin \gamma} (3 \gamma - 4 \sin \gamma \cos \gamma + \sin \gamma \cos^3 \gamma - \cos \gamma \sin^3 \gamma) \right]$$

Page 53. Line 3. The equation should be changed to

$$+ \frac{1}{4} \left[\sin^3 \gamma + \frac{\cos^2 \gamma \sin \gamma}{2} + \frac{\cos^4 \gamma}{2} \ln \left(\frac{\cos \gamma}{1 + \sin \gamma} \right) + \sin^4 \gamma \right]$$

Case V should repeat Case IV, and the leading coefficient

$$\frac{\pi}{2 \sin \gamma} \text{ should be changed to } \frac{1}{2 \sin \gamma} \text{ for Case V only.}$$

Page 60. Fig. IV-1(b). Add $\sigma = 28.4$ deg.

[†]Cord H. Link, Jr. "Problems in Computing Radiation Control Functions for Mark I." Arnold Engineering Development Center, Arnold Air Force Station, Tennessee. AEDC-TDR-63-206, February 1964. (Unclassified Report)

PROBLEMS IN COMPUTING
RADIATION CONTROL FUNCTIONS FOR MARK I

By
Cord H. Link, Jr.
Scientific Computing Services
Office of the Director of Engineering
ARO, Inc.
a subsidiary of Sverdrup and Parcel, Inc.

February 1964
ARO Project No. SM2105

ABSTRACT

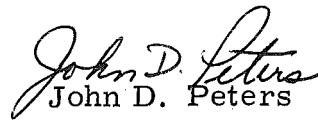
This report assembles the results of studies in the field of space flight thermal radiation simulation to provide a system to compute real-time information about the intensity and distribution of thermal radiation fields illuminating a vehicle in space. The details are limited to vehicles in near earth orbits, but the discussion is sufficiently generalized to indicate how transfer trajectories and alternate primary bodies may be incorporated. The time functions obtained may eventually control the sequencing of parameters in the Mark I aerospace environment simulator or at least provide an independent means to evaluate system performance when the simulator becomes operational.

PUBLICATION REVIEW

This report has been reviewed and publication is approved.



G. M. Arnold
Chief, Engineering Division
Space Systems Office



John D. Peters
Lt Col, USAF
Chief, Space Systems Office

CONTENTS

	<u>Page</u>
ABSTRACT	iii
NOMENCLATURE	vii
1.0 INTRODUCTION	1
2.0 THE GENERAL COMPUTER PROBLEM	4
3.0 SOLAR CONTROL AND ORBITS	
3.1 Orbit Definition	7
3.2 Orbit Calculations	8
3.3 Coordinate System	11
3.4 Orientation	12
3.5 Roll and Pitch	14
3.6 Orbits	18
3.7 Solar Bank Control	27
4.0 SECONDARY ILLUMINATION	28
4.1 Secondary Illumination Simulation	30
4.2 "Birdcage" Patterns and Matching	34
4.3 Illumination Integrals	40
4.4 Radiance Functions	46
5.0 CONCLUSIONS	47
REFERENCES	47
APPENDIXES	
I. A List of 7074 Programs Concerned with Mark I Illumination Simulation	49
II. Special Cases of Albedo Integral	50
III. Earth Radiance Integral	54
IV. Sample Profile	59

TABLES

1. Program Block Outline	5
2. Program Elements	7

ILLUSTRATIONS

Figure

1. The Simulation Problem	1
2. Illumination of Satellite	2
3. Typical Shapes and Properties	3

<u>Figure</u>	<u>Page</u>
4. Distinction between Rotational Quantities and Revolutional Quantities in Flight.	8
5. Calculation of Node Vectors.	9
6. Earth-Centered Inertial Coordinate System.	11
7. Orientation Types	13
8. Roll and Pitch Geometry	15
9. Roll and Pitch Functions of Orbit Position	17
10. Roll Rate Editing	17
11. Eclipse Geometry	19
12. Eclipse Test	20
13. Orbit Coordinate Angles	22
14. Orbit in Space and in Plane Illustrating the Euler Angles, Ω , θ_i , ω	22
15. Secular Perturbations Caused by Earth Oblateness	25
16. Geometry for Study of Longitudinal Flux Distributions	30
17. Longitudinal Flux Distributions for Line Source Arrays as Function of Distance from Line	32
18. Approximate Effect of Reflecting End Baffles on Longitudinal Flux Distribution for a Single Line Source Element	33
19. Integral Profile Matching.	35
20. Profile Matching with Integrals	36
21. Six-Point Profile Matching	37
22. Profile Matching at Six Points Only	38
23. Solid Angle Geometry for Albedo and Earth Radiance Calculation	41
24. Coordinate Relations for Albedo and Earth Radiance Calculation	42
25. Albedo-Radiance Integration Coordinates.	43
26. Area Elements for Cylinder-Cone	44

(SCAN NOTE - PAGE IS BLANK IN ORIGINAL DOCUMENT)

J	Earth gravitational potential constant
L	Angular momentum
L_A	Vehicle rotational angular momentum or turning axis
L_V	Orbital angular momentum
ℓ	Length of line segment
M	Mean anomaly
M_e	Mass of earth
N	Normal vector or nodal vector or no. of line segments
N_A	Nodal vector reference for angle ϕ_A
N_o	Nodal vector reference for angle ϕ_V
N_V	Normal vector to vehicle surface
n	Mean motion
P	Vector projection of R in plane perpendicular to S_i
p	Pitch angle of vehicle relative to plane perpendicular to S_i
R	Distance from line source
R_e	Position vector on earth's surface
R_V	Position vector for vehicle
r	Polar distance on $x^* y^*$ plane
r_e	Earth radius
r_V	Magnitude of R_V
S	Segment spacing (on center), line source
S_i	Unit vector of solar position
S_K	K^{th} region of area for integration
T	Period of motion
T_V	Orbital period, Keplerian orbit
t	Time
t_p	Time from pericenter
V	Velocity vector
v	Magnitude of V
W	Total flux per unit length of radiating line segment

x_a	Coordinate of target for line sources
x_i	Coordinate for line segment
x^*, y^*	Rectangular coordinates in orbit plane
x, y, z	Right-handed, earth-centered, inertial, rectangular coordinates
α	Azimuth angle
α_N	α of normal vector
β	Nadir angle
β_N	β of normal vector
γ	Horizon angle
θ	Angle between plane of motion and S_i
θ_A	θ from A, A plane
θ_e	Angle between R_e and S_i
θ_i	Angle to i^{th} line segment point, or inclination of orbit plane to equatorial plane
θ_S	θ from R, V plane
θ_V	Angle between R_V and S_i
μ	GM_e , constant of motion
ξ	Angle from normal for incident radiation at vehicle
ρ	Roll angle of vehicle
ρ_e	Distance between vehicle and point on earth's surface
σ	Cone half angle
τ	Path angle defined by $R_{V_1} \times V_1 = \sin \tau$
ϕ	Turning angle or angle between R_V , R_e
ϕ_A	Turning angle of A from N_A
ϕ_V	Turning angle of R from N_o
ψ	Angle from normal for reflected or emitted radiation at earth's surface
Ω	Angle of line of nodes from x axis in equatorial plane
ω	Angle from line of nodes to pericenter in orbit plane or solid angle

$\bar{\omega}$	Replaces $\Omega + \omega$ when $\theta_i = 0$, since then line of nodes is not defined
Υ	First point in Aries, vernal equinox

SUBSCRIPTS

l	Unit vector
A	Relates to vector A
e	Relates to earth
N	Relates to surface normal
O	Initial value
S	Relates to sun
V	Relates to vehicle
x,y,z	Vector components

1.0 INTRODUCTION

This report assembles the results of studies performed by Scientific Computing Services, ARO, Inc., Arnold Engineering Development Center (AEDC), Air Force Systems Command (AFSC), in the field of space flight thermal radiation simulation to provide a system to compute real-time information about the intensity and distribution of thermal radiation fields illuminating a vehicle in near earth orbit, in transfer trajectories, and in orbit about any primary body. The time functions so obtained may eventually control the sequencing of parameters in the Mark I aerospace environment simulator. They will at least provide an independent means of evaluating performance of the actual system when it becomes operational.

This report is mainly limited to near earth orbits, but discussion is sufficiently generalized to indicate how transfer trajectories and alternate primary bodies may be incorporated. We shall first outline the simulation problem, then sketch a possible comprehensive computer program, and, finally, go into details of the arithmetic involved for a variety of options that may be included. Appendix I is a list of the 7074 programs at AEDC concerned with Mark I illumination simulation.

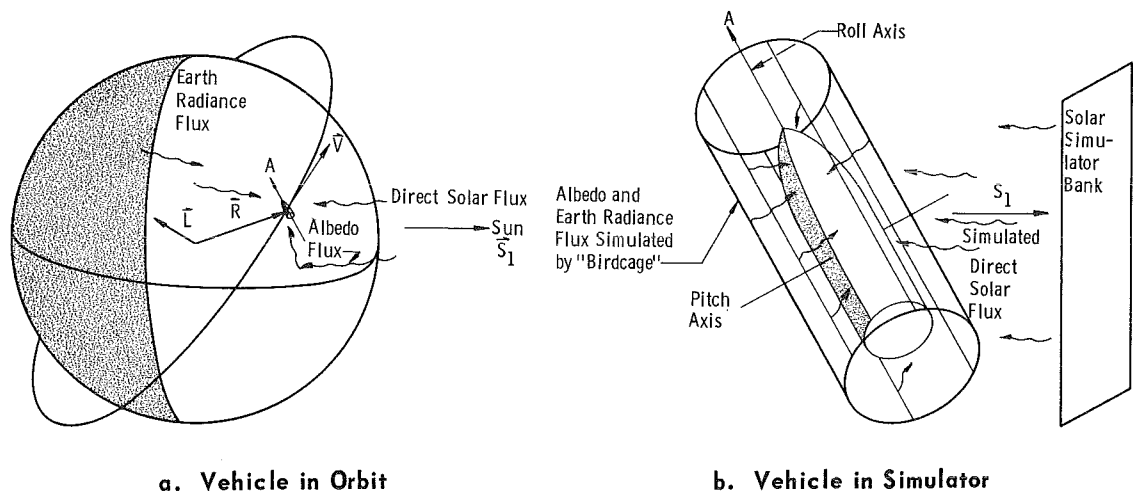


Fig. 1 The Simulation Problem

A space vehicle is exposed to direct solar illumination except when eclipsing occurs because of shadowing by a primary body (Fig. 1). If the vehicle is sufficiently close to the primary body, it may receive significant additional illumination of two kinds. The primary body reflects

Manuscript received August 1963.

some fraction of the direct solar radiation incident on it (Albedo) and absorbs and re-emits additional thermal radiation (planetary radiance). We will take the earth to be the primary body in what follows; the application to other primaries is generally obvious.

For a near earth orbit, the direct solar radiation intensity is taken to be the "solar constant", invariant with orbital position. The direct solar illumination of the vehicle depends on its attitude relative to the sun and vanishes during eclipse. The albedo radiation depends on effective surface properties of the primary, assumed uniform for a particular primary, and rather complexly, on the detailed vehicle-primary-sun configuration. It vanishes during eclipse. The earth radiance illumination depends on the properties of the primary body, on the vehicle-primary configuration, and continues during the eclipse.

The paragraph above describes the illumination field in the neighborhood of an orbiting vehicle. The thermal input to a vehicle depends upon its shape, its orientation in the illumination field, and its surface properties relative to the spectral content of the radiation (Fig. 2).

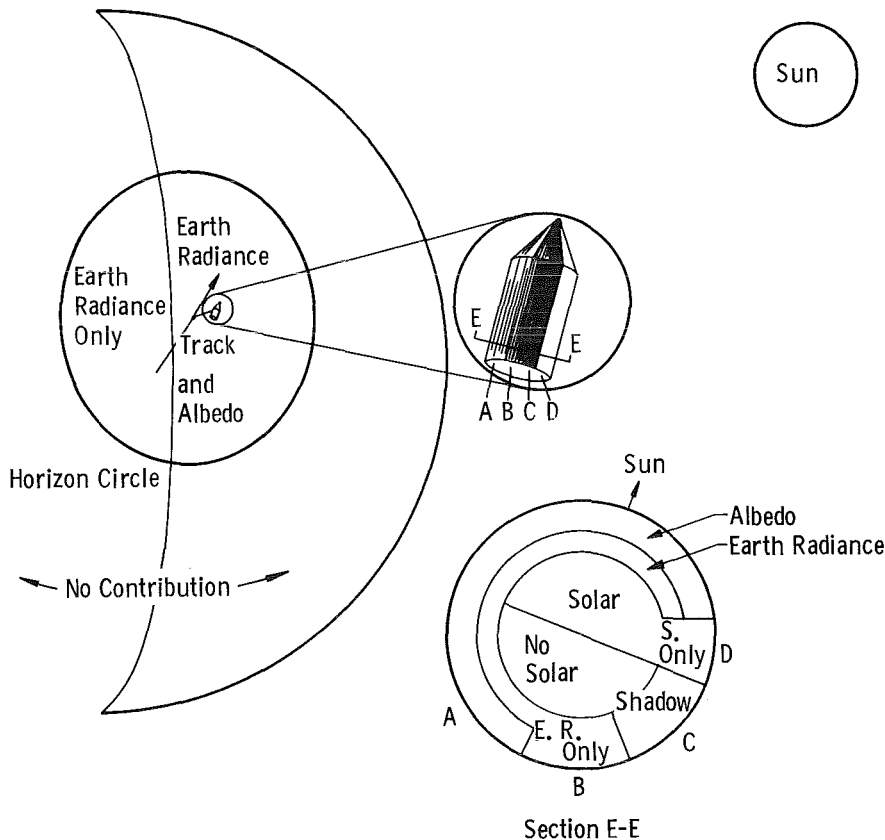
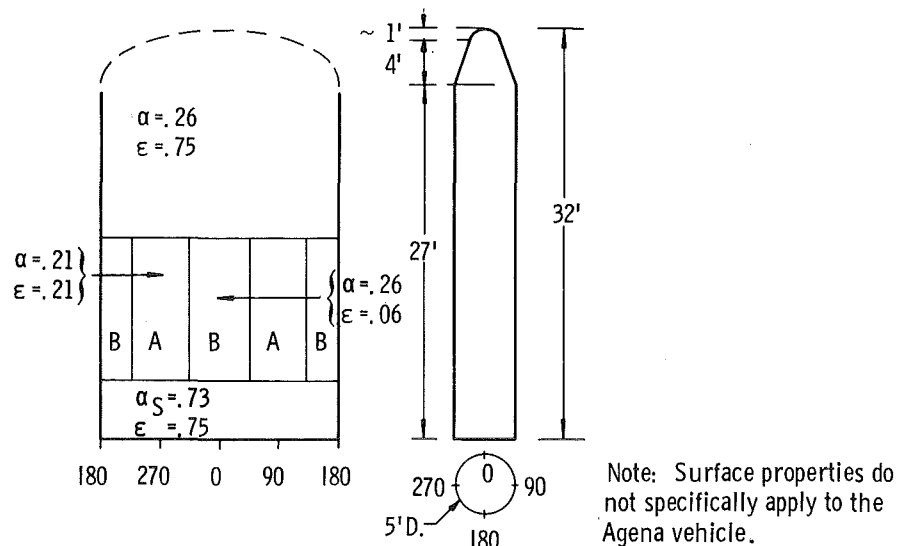
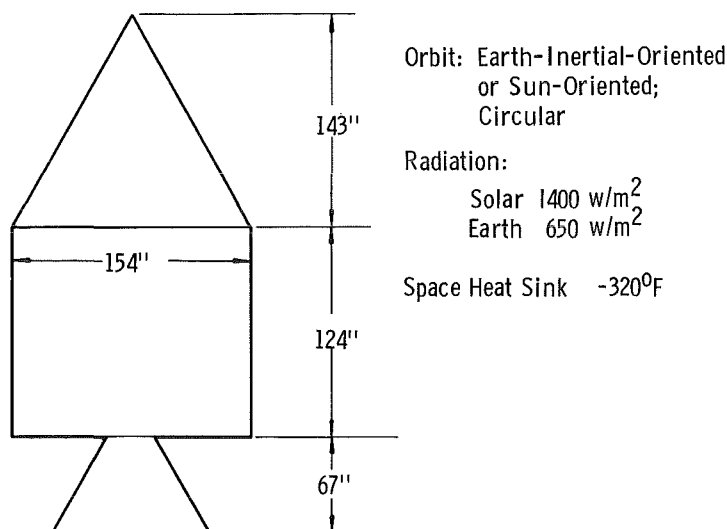


Fig. 2 Illumination of Satellite

The illumination field becomes the thermal input to the vehicle at its surface. Consequently, the thermal input depends on the particular point on the vehicle (Fig. 3). Any surface element may have distinct thermal properties and may be exposed to all three, two, one, or none of the illumination components.



a. Agena Type



b. Apollo Type

Fig. 3 Typical Shapes and Properties

This complex interdependence is to be simulated in the Mark I chamber, possibly synchronized with other simulation parameters, such as vacuum conditions and propulsion loads. Solar radiation will

be simulated by the "solar bank", an extensive planar array of optical elements to provide highly directional (collimated) illumination of essentially true solar spectral composition. Albedo and earth radiance are to be simulated by an open "bird-cage," essentially several linear arrays of heating elements with roughly parabolic cylindrical reflectors. The solar bank is fixed in the chamber. The vehicle is mounted on a horizontal pitch axis so that its pitching plane bisects the solar bank. The vehicle rolls about an axis that is free in the pitch plane. The bird-cage array pitches with the vehicle but does not roll. The whole range of possible vehicle-primary-sun configuration is thus to be simulated by pitch and roll of the vehicle and by shifting the illumination pattern of the birdcage.

Eclipsing means simply extinguishing the solar bank and the albedo component of the birdcage illumination pattern but leaving the earth radiance component turned on.

A further interdependence condition is imposed by the Mark I chamber itself. The system of solar bank, vehicle mount, and birdcage is contained in a large vacuum vessel whose dark refrigerated inner walls simulate the heat sink of space. The large area of the solar bank replaces some cold wall area, and the solar bank is the principle source of the heat load on the wall refrigeration system. Consequently, it is desirable that any element of the solar bank shall be turned off whenever its collimated beam will not strike the vehicle. The pattern of "on" solar bank elements depends on vehicle-sun attitude and on vehicle shape.

This report will attempt to show how the control parameters may be computed and inter-related as required by the nature of any particular test. The actual use of the time-sequenced parameters by the control hardware, an instrumentation problem, is beyond the scope of this report.

2.0 THE GENERAL COMPUTER PROBLEM

Since simulation takes place in real time, and all control parameters are to be computed in advance, it is highly desirable that the computing time be a small fraction of the corresponding real time for a test of any significant duration. This is especially true if the computing is done on a general purpose machine which has additional workloads. Two ways can be exploited to make the computer-to-real-time ratio more favorable. One may plan to use a faster computer or to simplify the calculations, at a reduction of realism in simulation.

At the outset, the conditions to be simulated may be chosen so that they compute simply. An example is a circular near-earth orbit with all parameters fixed once and for all, adequate for very few revolutions, over a time interval less than a day, after which significant changes must be introduced if the simulation is not to degrade seriously.

At a more advanced level, for sophisticated simulation, the computer time rises because of the form of equations which must be evaluated. Here it is possible to introduce approximating functions which compute faster.

These considerations will be dealt with as they arise in the following pages. In the past, our work has been based on the idea that we strive for the highest realism until it proves impractical. We have then at least a measure of the cost of coarser approximation in loss of realism. The geometry of the simulation forces a number of approximations; our lack of certain detailed knowledge and our inability to handle massive detail force further approximations.

The most feasible program appears to be one consisting of two or three blocks, as required by the size of the problem and computer storage needed (see Table 1).

In the first block, all orbit calculations are performed, and from them are found the roll, pitch, their rates, and the existence of either the eclipse condition or the excess roll rate condition (these two cannot occur together in principle). Also, in case of monotonic pitch, revolutions in pitch are counted.

TABLE 1
PROGRAM BLOCK OUTLINE

CALL BLOCK 1

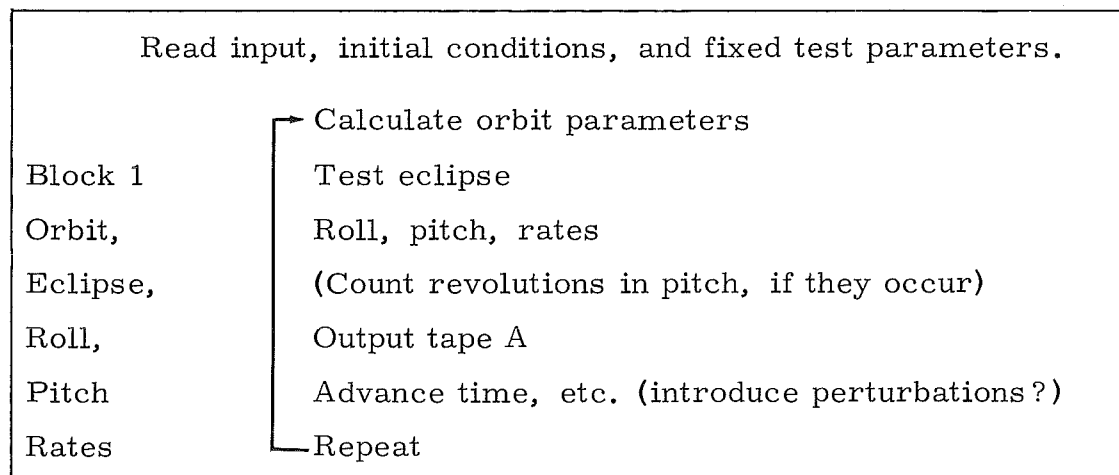
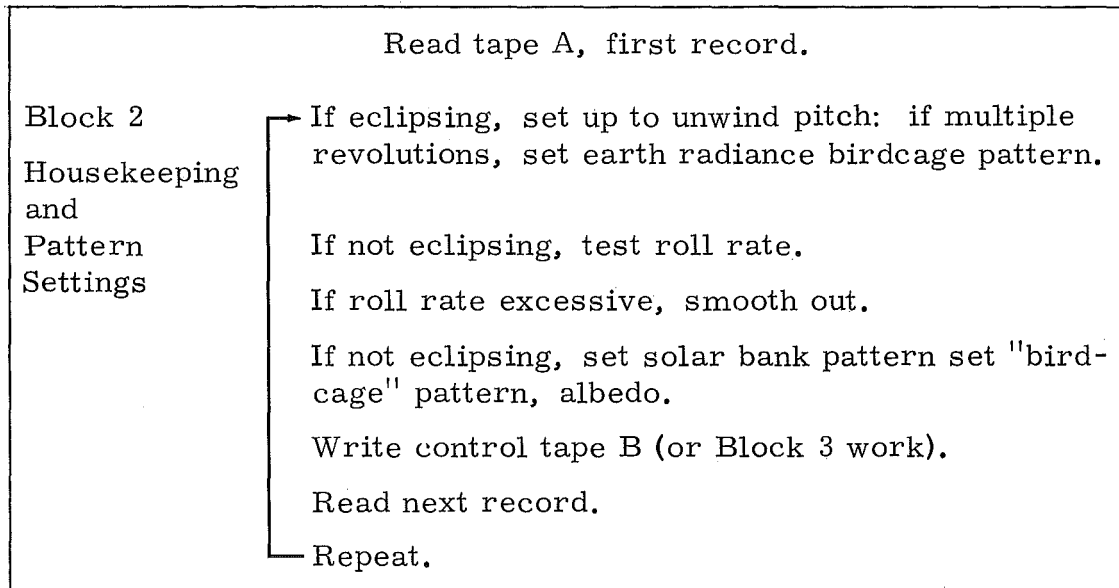
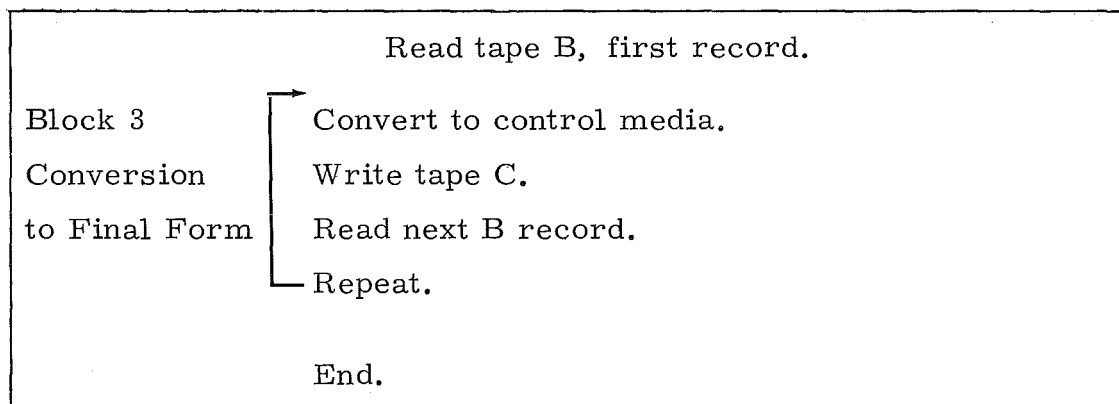


TABLE 1 (Concluded)

CALL BLOCK 2



CALL BLOCK 3



In the second block, the roll function is smoothed if it has excessive rate, and the illumination array patterns are reset. During the eclipse condition, the monotonic pitch condition may indicate that pitch be backed off one or more revolutions rapidly to unwind control cables. This condition occurs only when eclipsing times are maximum. Part of this block may have to be delayed to the next block.

Block three is a simple conversion routine to prepare the final control media, either tape or cards, in the format required by the control hardware.

Blocks in which computing predominates are built up from program elements for which options are to be selected for specific tests (see Table 2.)

TABLE 2
PROGRAM ELEMENTS

I. THE ORBIT

A. Earth Centered

1. circle
2. ellipse
3. exact

B. Perturbations

4. diurnal motion of the sun
5. oblate earth perturbations
6. other body perturbations

C. Other Orbits

7. orbits about other primaries
8. transfer orbits
9. launch-recovery trajectories

II. SOLAR SIMULATION

A. Roll, Pitch, Rates

B. Eclipsing

C. Editor for Mechanical Limits

D. Solar Bank Pattern Control

III. SECONDARY ILLUMINATION

A. Albedo-Earthshine Field

B. "Birdcage" Pattern Control

3.0 SOLAR CONTROL AND ORBITS

3.1 ORBIT DEFINITION

It is intuitively desirable to think of an orbit as a closed curve, a circle, or an ellipse, although this may be far from realistic. We define the "osculating ellipse" as that ellipse which instantaneously

matches the actual orbital path and consider the orbit in this manner. In the absence of perturbations, simple one body central force motions, the osculating ellipse has constant parameters and provides an ideal stationary description.

In the presence of perturbations, we may think of the osculating ellipse as being slowly changed in shape, in orientation in its plane, and its plane slowly changing orientation in space. These changes are mostly oscillatory; only those caused by non-sphericity of the earth provide significant unidirectional changes. We will look at this later.

3.2 ORBIT CALCULATIONS

Whatever mathematical model is used to calculate the orbital motion, it must produce certain vector quantities or their equivalents. We require the position vector \vec{R}_V , velocity vector \vec{V} , and perhaps the vehicle axial vector \vec{A}_1 , which defines the axis of the spin (roll axis), and its time derivative $\dot{\vec{A}}$. (Note: subscript 1 means unit vector.) (See Figs. 4 and 5).

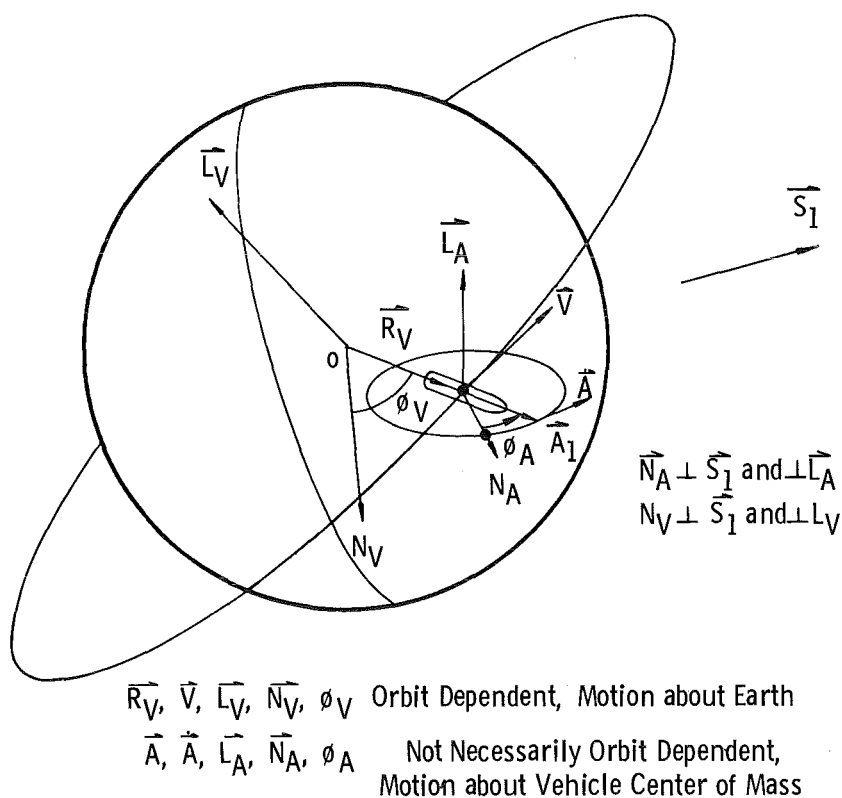


Fig. 4 Distinction between Rotational Quantities and Revolutionary Quantities in Flight

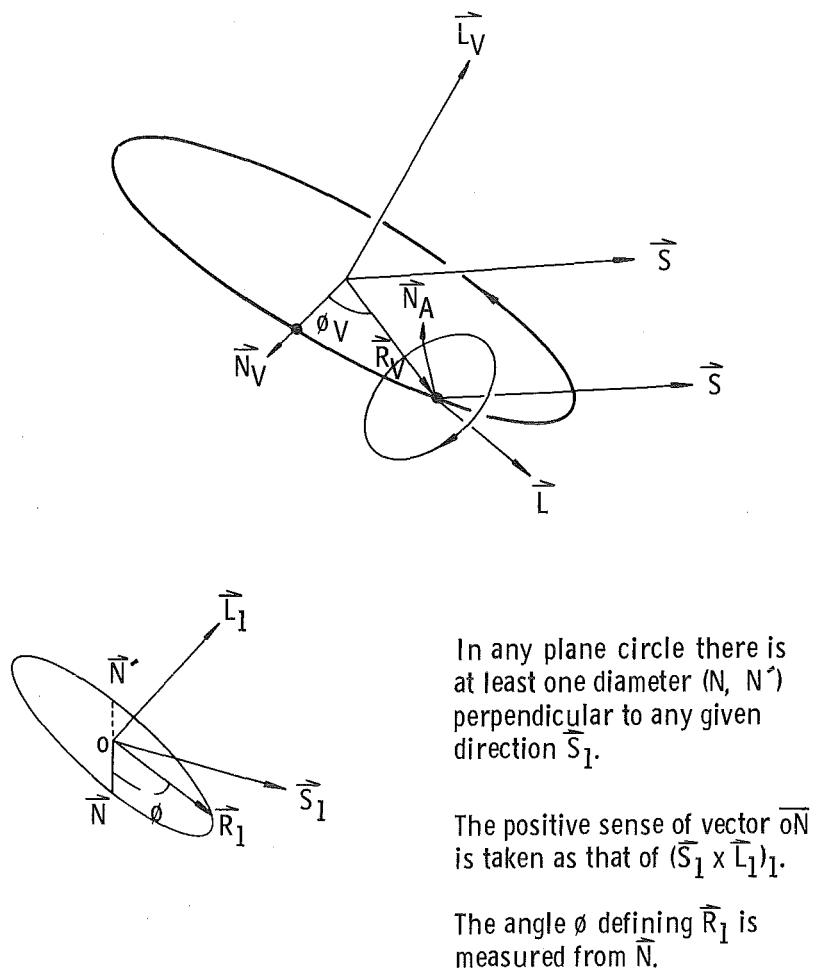


Fig. 5 Calculation of Node Vectors

For any orbital motion, the first immediately useful information obtainable is the eclipsing interval. Eclipsing depends only on the position, not the attitude, of the orbiting body relative to the earth's shadow. The earth is assumed to be a sphere, devoid of atmosphere, casting a right circular cylindrical shadow, geometrically defined (Fig. 11, page 19).

If \vec{R}_V is the position vector of the orbiting vehicle, R_e , the earth radius, and \vec{S}_1 is a unit vector from earth to sun, we find the projection \vec{P} of \vec{R}_V on a plane perpendicular to \vec{S}_1 , and test the magnitude of the projection against R_e . If $|\vec{P}| < R_e$ and if the vehicle is on the aphelion limb of the orbit, the vehicle is in eclipse. The last condition is more simply stated as the requirement that $\vec{R}_V \cdot \vec{S}_1$ be negative. The dependence of eclipse interval on orbit parameters is detailed in Ref. 1.

The eclipse indicator may be used later to bypass all albedo calculations, to turn off the solar bank entirely, and to relieve the constraint

on number of revolutions in pitch angle. This last situation occurs for orbits where the vehicle roll axis \vec{A}_1 passes through the sun, for when this happens the pitch is monotonic rather than oscillatory, as will be seen below.

The vector product $\vec{R}_V \times \vec{V}$ defines the orbital angular momentum vector (per unit mass) \vec{L} and hence defines the instantaneous plane of the orbit. The vector product $(\vec{A}_1 \times \dot{\vec{A}})_1$ defines the axis about which the vehicle is turning its axis \vec{A} at the instant, and this is the vehicle angular momentum vector \vec{L}_A (if there is no spin about \vec{A}).

For some modes of orbital flight, the two vectors, \vec{L} and \vec{L}_A , coincide. Hence the turning axis (in the direction of \vec{L}_A) may be obtained directly from the orbital vectors \vec{R} and \vec{V} . For other modes of flight, \vec{L}_A may not be determinate from the orbit but must be specially given.

Now if \vec{S}_1 is a unit vector pointing to the sun, the angle θ_S between orbit plane and sun direction is obtained from

$$\vec{S}_1 \cdot \vec{L}_1 = -\sin \theta_S$$

and a nodal vector from which orbital angles are measured is

$$\vec{N}_0 = (\vec{S}_1 \times \vec{L}_1)_1 \quad (\text{Fig. 5})$$

The angle ϕ_V between \vec{R}_V and \vec{N}_0 is then obtained from

$$\cos \phi_V = \vec{R}_{V1} \cdot \vec{N}_0$$

Similarly, at any instant the vehicle axis vector \vec{A} is turning about the vector \vec{L}_A in a plane inclined at angle θ_A defined by $\vec{S}_1 \cdot \vec{L}_A = -\sin \theta_A$ to the sun direction \vec{S}_1 . \vec{A}_1 has turned through angle ϕ_A from a nodal direction $\vec{N}_A = (\vec{S}_1 \times \vec{L}_A)_1$ such that

$$\cos \phi_A = \vec{A}_1 \cdot \vec{N}_A.$$

As defined, the nodal vectors \vec{N}_0 and \vec{N}_A lie in their respective turning planes and are perpendicular to the sun vector \vec{S}_1 as well as to their respective \vec{L} and \vec{L}_A . If the angular momentum \vec{L} and \vec{L}_A always coincide in direction, then \vec{R}_V , \vec{V} , \vec{A} and $\dot{\vec{A}}$ are coplanar, the node vectors \vec{N}_0 and \vec{N}_A coincide and \vec{A} and \vec{R}_V are related by

$$\phi_A = \phi_V + \tau$$

where

$$\tan \tau = \left| \frac{\vec{R}_V \times \vec{A}}{\vec{R}_V \cdot \vec{A}} \right|$$

The distinction between the pairs of vectors \vec{R}_V, \vec{V} and $\vec{A}, \dot{\vec{A}}$ is as follows: \vec{R}_V and \vec{V} are orbit descriptors, serving to determine vehicle location in orbit, essential in establishing the eclipse condition, and for locating the vehicle position relative to the Albedo source, the sunlit hemisphere of the earth. The vectors \vec{A} and $\dot{\vec{A}}$ are vehicle attitude descriptors, governing its exposure to direct solar radiation and its attitude toward the earth for both Albedo and earthshine radiation. For some orientations of the vehicle in orbit, these vector sets are functionally coupled, and only one needs to be developed.

3.3 COORDINATE SYSTEM

Although we use vector notation for freedom from particular coordinate systems, numerical computations do require vector components which are dependent on the coordinate system selected.

In the following, the fundamental coordinates are geocentric, non-rotating, orthogonal axes defined as follows. The z-axis points north, parallel to the earth's axis. The x-axis points to the vernal equinox of some particular date,* and the y-axis is so located as to form a right handed system (Fig. 6). As required for clarity or efficiency, other coordinate systems will be defined and introduced.

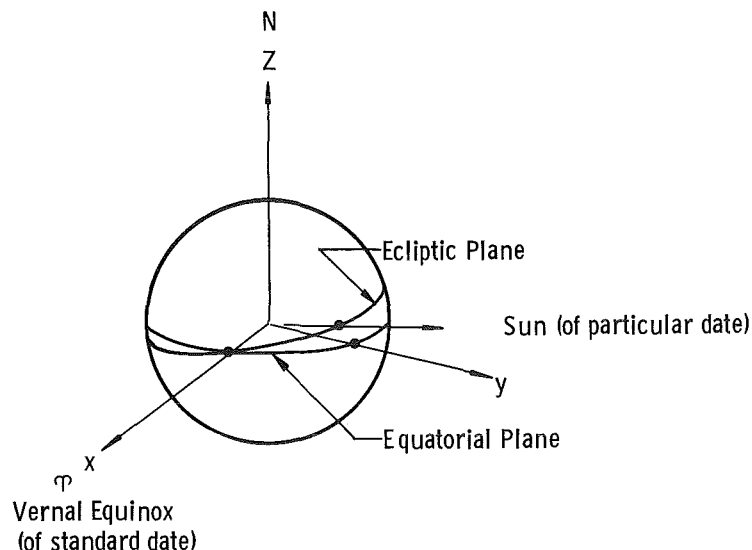


Fig. 6 Earth-Centered Inertial Coordinate System

*The date of reference for particular tables; for example, "the mean equinox of 1950.0."

We use the geocentric inertial system so that astronomical data may be used, directly from "Ephemeris" tables (Ref. 2). For any degree of realism in computing attitude of a vehicle to the sun, we require coordinates of the sun position relative to the earth. For high realism other body coordinates will be needed. These are available on "Themis" magnetic tapes (Ref. 3).

Within the Mark I chamber the coordinates for the motion are pitch p and roll ρ , angles defined by the mechanical construction as previously described. Depending upon the constraints of the vehicle motion, the sun angle θ and vehicle turning angle ϕ will be defined in slightly differing terms, and from these angles, roll and pitch are calculated.

3.4 ORIENTATION

By vehicle orientation, we mean certain fixed constraints of relations between the vehicle axes and directions in space or to other bodies. There are five commonly conceived orientations (Fig. 7):

1. A vehicle which has no motion about its center of mass is space oriented. It may have only one axis fixed in direction, typically the spin axis for a spin stabilized missile.
2. A vehicle may have a fixed orientation relative to the earth, for example, a photo-reconnaissance vehicle, and is said to be earth oriented.
3. A minimum of solar radiation input to an orbiting vehicle is obtained when minimum cross section area is exposed to the sun, a solar orientation.
4. The roll axis of the vehicle may be maintained coincident with the velocity vector, tangent to the orbit, thus called tangent oriented. This is the most common concept of orbital flight orientation.
5. If the orbital angular velocity vector and the vehicle angular velocity vector coincide and are equal (i. e., the rotation period equals the revolution period and the motions are coaxial), this may be called an angular momentum orientation. This will be also tangent orientation for a circular orbit and will be earth oriented.

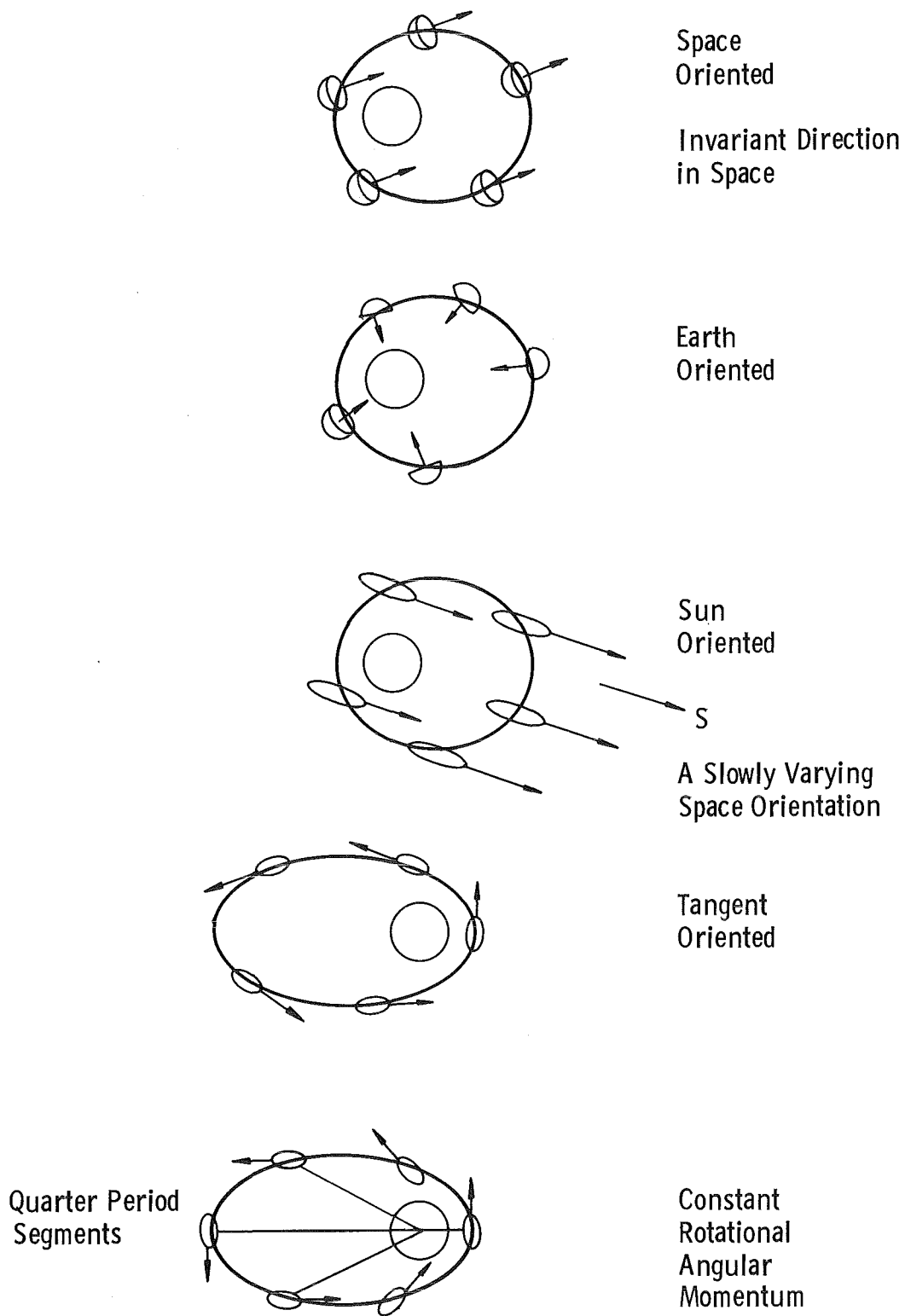


Fig. 7 Orientation Types

From these examples we see that orientation can be partly or completely specified by stating the fixed relation between one or more axes of the vehicle and a fixed space direction, a direction to another body, or relative to definite directions, in one, two, or three dimensions. A vehicle employing thrust for attitude control may have continually varying orientation.

If we are to obtain analytic descriptions of orbital flight, it is desirable to assume a definite orientation to hold throughout the time interval of interest. In the following, we shall assume tangent orientation without spin. We will remain aware of the fact that a real flight with attitude control may be piecewise analytic but not describable in advance, unless scheduled accurately. In that case, the ordinary laws of mechanics can be applied to determine the complete history of orientations in advance.

Tangent orientation means that the vehicle axis lies in the plane of the orbit. For a circular orbit, the axis vector \vec{A} will be perpendicular to the position vector \vec{R}_V . Hence ϕ_A will be 90 deg ahead of ϕ_V . For elliptical orbits, the axis vector will be perpendicular to the position vector only at perigee and apogee. From perigee to apogee the vehicle is gaining altitude, the axis is above the horizontal; during the passage apogee to perigee, it is below the horizontal. For ordinary Keplerian orbital motion, this angle of elevation or depression is easily calculated, so that the vehicle axis vector \vec{A} may be found from the orbit position vector \vec{R}_V .

Regardless of orientation, it is always necessary to compute the progress of the vehicle along the orbit, if only to test for and simulate eclipsing. The orbit position also enters Albedo calculations.

3.5 ROLL AND PITCH

We shall calculate the Mark I control parameters roll and pitch from the angles ϕ_A and θ_A . At the outset we see that the vector \vec{A} corresponds, not to a particular axis in the vehicle, but to an axis determined by the vehicle mounting in the Mark I cell. The vector \vec{A} is the cell-defined roll axis, and obviously the reference direction for roll can be anywhere in the vehicle, as long as it is perpendicular to \vec{A} . We assume the convention that the zero pitch and roll position is the original mounting configuration in the cell. The initial pitch and roll for the motion depend on the earth-sun-vehicle configuration at injection into the orbit.

A vehicle on which no torques act has constant rotational angular momentum \vec{L}_A (Fig. 8). If this vector is aligned with the sun direction,

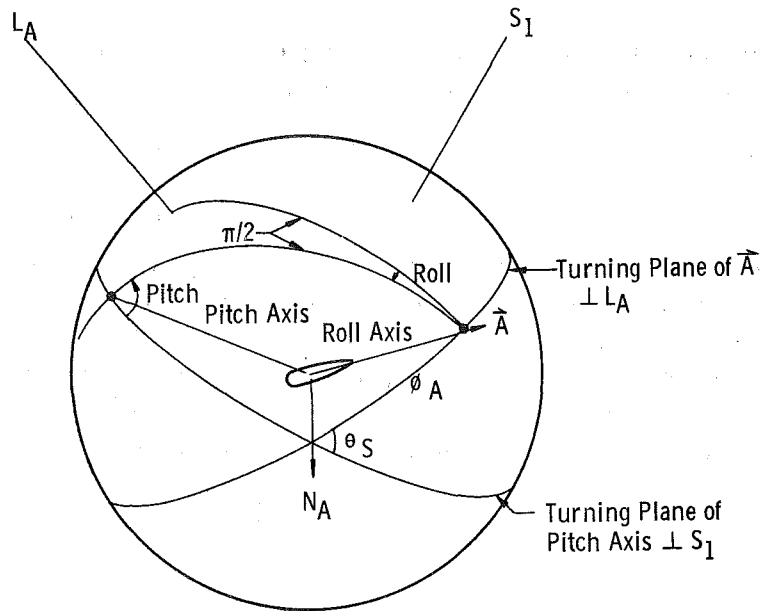


Fig. 8 Roll and Pitch Geometry

$\vec{L}_A = -\vec{S}_1$, the plane of the motion is perpendicular to the sun direction. Roll and pitch are constant in this case, and it is convenient to take this configuration as defining the zeros of roll and pitch. This corresponds to a circumpolar orbit, tangent oriented vehicle, crossing north over the equator at sunrise. By the definition of solar inclination angle θ_A , this case means $\theta_A = \pi/2$. If we let $\theta_A = 0$, the plane of the motion contains the sun vector \vec{S}_1 . Any time the vector \vec{A}_1 coincides with $\pm\vec{S}_1$, the roll ρ is undefined. At such critical points we have an operating option: we may allow pitch p to increase monotonically; or we may reverse the pitch direction and change the roll by 180° . In the first option roll is unchanged, and pitch can go through several complete revolutions before mechanical restrictions force us to "unwind". In the second option, roll can be flipped only as fast as the roll drive permits (about 1 rpm), but pitch is then limited to the range $-\pi/2, 0, \pi/2$, and there is no unwinding problem. All this applies only for $\theta_A = 0$. If the sense of positive pitch is toward the sun, with zeroes as described above, we have pitch p and roll ρ given by spherical trigonometry in the forms

$$\sin p = \cos \theta_A \sin \phi_A$$

$$\sin \rho = \cos \theta_A \cos \phi_A / \cos p.$$

From these expressions we see that $\sin p$ is limited in amplitude to $\cos \theta_A$ and is otherwise simply proportional to $\sin \phi_A$: as ϕ_A goes through a complete revolution, p oscillates smoothly between $\pm(\pi/2 - \theta_A)$.

If $\theta_A = \pi/2$, the oscillation has zero amplitude, i. e., $p = 0$. Finally if $\theta_A = 0$, we have simply $p = \phi_A$ or, optionally

$$\begin{aligned} \text{For } \phi_A = 0, \pm \pi/2, \quad p &= \phi & dp &= d\phi \\ \phi_A = \pi \pm \pi/2 \quad p &= \pi - \phi & dp &= -d\phi \end{aligned}$$

Examining the expression for ρ in the same way, we see ρ is oscillatory in ϕ_A with amplitude determined by θ_A . We note that $\theta_A = \pi/2$ gives $\cos \rho \cos p = 1$, requiring $\rho = 0$ and $p = 0$, and $\theta_A = 0$ gives $\sin \rho = 1$, $\rho = \pi/2$. At intermediate θ_A , $p = 0$ gives $\sin \rho = \cos \theta_A \cos \phi_A$. When both are oscillatory, ρ is $\pi/2$ out of phase with p . When θ_A is zero, and we choose the limited pitch option above, we have for ρ these conditions:

$$\begin{aligned} \text{when } 0 < \phi_A < \pi, \quad \rho &= \pi/2 \\ \pi < \phi_A < 2\pi, \quad \rho &= -\pi/2 \end{aligned}$$

These relations are also implied in

$$\cos \rho \cos p = \sin \theta_A$$

for when θ_A vanished, since p is simply ϕ_A or $\pi - \phi_A$, except for $\phi_A = \pm \pi/2$, we must have ρ identically $\pm \pi/2$. And when $\theta_A = \pi/2$, we must have both ρ and $p = 0$ or π .

We now examine the roll and pitch rates $\dot{\rho}$ and \dot{p} . By differentiating and substituting identities we find

$$\begin{aligned} \dot{p} &= \sin \rho \dot{\phi}_A \\ \dot{\rho} &= -\tan p \cos \rho \dot{\phi}_A \end{aligned}$$

where $\dot{\phi}_A$ is the instantaneous angular velocity of rotation of vector \vec{A} about its axis \vec{L}_A . This form ignores any contribution caused by precession which would give terms in $\dot{\theta}_A$. Such terms are normally much smaller than those in $\dot{\phi}_A$.

We see that $\dot{\rho}$ has a singularity if $p = \pm \pi/2$. From earlier arguments, this can only occur when $\theta_A = 0$, but for $\theta_A = 0$, $\rho = \pm \pi/2$, $\cos \rho$ vanishes and $\dot{\rho}$ is indeterminate. For θ_A small ρ takes on large values at $p = \pm \frac{\pi}{2}$ (Fig. 9). The Mark I mechanical limit of 1 rpm means that we smooth across the steep portion of the graph of roll versus ϕ_A , with a line or curve having slope not exceeding 1 rpm. Except in extreme instances, less time is involved in this smoothed portion if we delay smoothing until required, rather than try to anticipate it (Fig. 10), and the computer programming is considerably simplified.

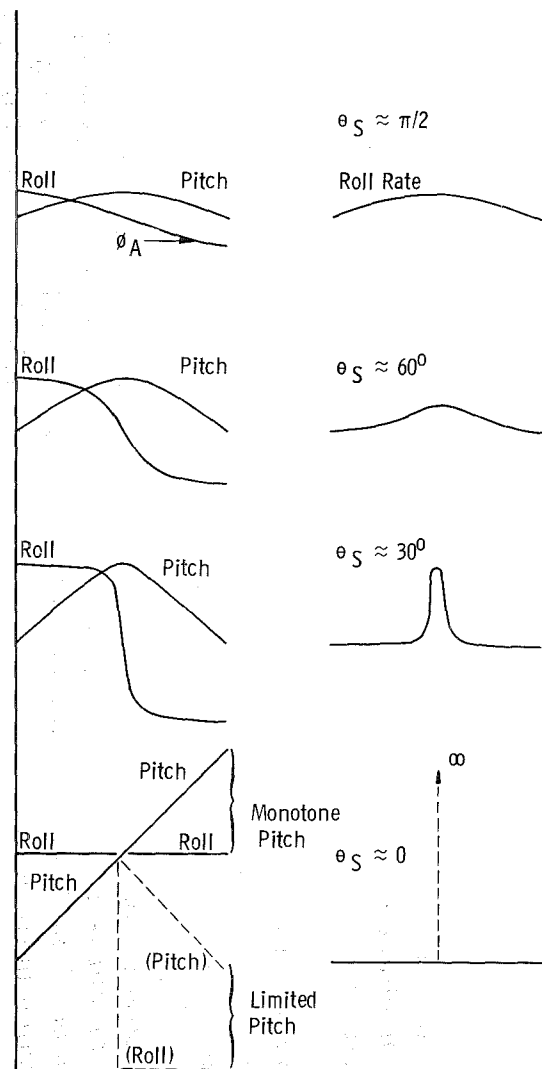
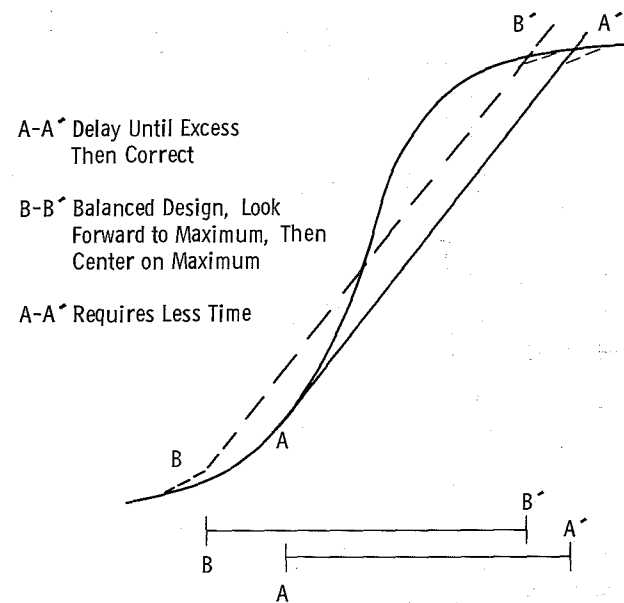
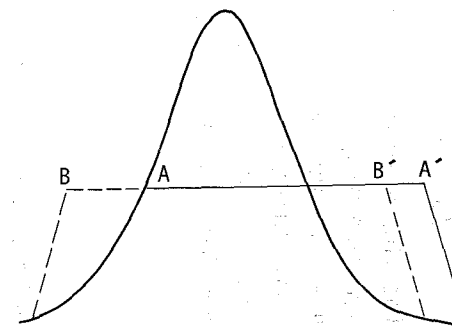


Fig. 9 Roll and Pitch Functions of Orbit Position



a. Roll



b. Roll Rate

Fig. 10 Roll Rate Editing

This condition, roll rate exceeding the mechanical limit, must be identified when computing roll and pitch. The infinite values do not actually occur since they are absorbed by the pitch becoming monotonic rather than oscillatory, or optionally, by reversing the sign of \dot{p} as stated earlier and flipping ρ through π , which, of course, is also subject to the 1-rpm limit. At worst, only 1/2 min suffices to switch over. This can occur twice per revolution in ϕ_A , and its importance is thus dependent on ϕ_A . For tangent-oriented orbital flight simulation, we have the excess rate condition occupying one minute or less out of the orbit period of (nominally) 90 min or more.

The smoothing of the roll function to avoid excess roll rate will be done by an editing program block. As the flight advances, roll, pitch, and rates are computed, roll rate is tested and, if excessive, an indicator is turned on. All this occurs in the first program block. The editing program block will scan for the excess roll rate indicator and, when it is found, will compute roll values from the smoothing line until the rate is again within the allowed range.

In the next section, we shall follow the calculation for the simplest kind of orbital flight model.

3.6 ORBITS

3.6.1 Circular Orbit, No Perturbations

In uniform rotational motion, we have the progress around the orbit, through central angle ϕ_V ,

$$\phi_V = \phi_{V_0} + \frac{2\pi(t - t_0)}{T_V}$$

where ϕ_{V_0} is the initial angle, t_0 is the initial time, T_V is the orbit period.

$$T_V = 2\pi \sqrt{\frac{r_V^3}{G M_e}}$$

with r_V the orbit radius, G the universal gravitation constant, and M_e the mass of the central body.

We assume tangent orientation; hence the path angle $\tau = \pi/2$, and the roll axis vector \vec{A} turns through angle ϕ_A ,

$$\phi_A = \phi_V + \pi/2$$

The node vectors coincide, $\vec{N}_A = \vec{N}_V$, as do the angular momenta, $L_{V_1} = L_{A_1}$ and the planes of the motions so that $\theta_V = \theta_A$. We assume

that injection into orbit (time to) occurs at sunrise at a latitude equal the sun declination of date, and hence, at the nodal point, and at an altitude h such that $h = r_v - r_e$ (r_e is earth radius). We define the horizon angle γ by

$$\sin \gamma = r_e / r_v$$

an important quantity in secondary illumination. Then eclipsing occurs between ϕ_v points (Fig. 11):

$$3\pi/2 \pm \Delta\phi \quad \text{if} \quad 0 < |\theta_v| < \gamma$$

or

$$\pi/2 \pm \Delta\phi \quad \text{if} \quad \pi - \gamma < |\theta_v| < \pi$$

and

$$\Delta\phi = \sin^{-1} \left[\frac{\sin^2 \gamma - \sin^2 \theta_v}{\cos \theta_v} \right]$$

This is equivalent to the earlier test expressions

$$\vec{R}_v^2 - (\vec{R}_v \cdot \vec{S}_1)^2 < R_e^2 \quad \text{and} \quad \vec{R}_v \cdot \vec{S}_1 < 0$$

required for eclipsing (Fig. 12).

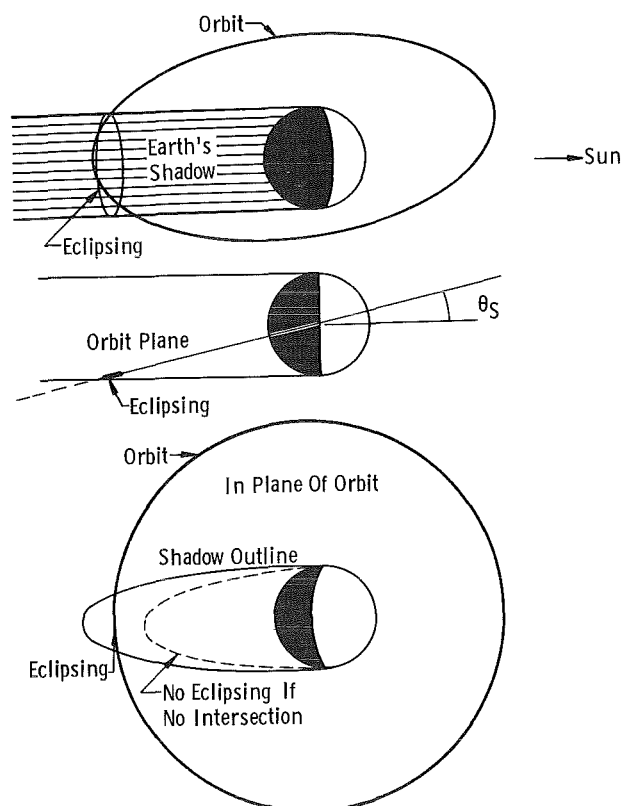


Fig. 11 Eclipse Geometry

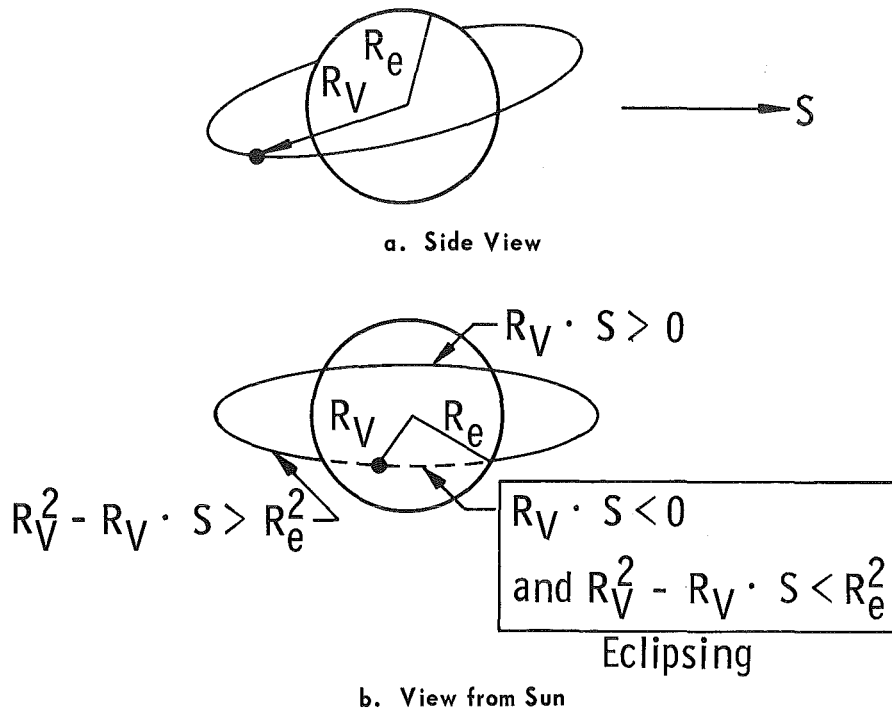


Fig. 12 Eclipse Test

In the circular orbit, the fraction of time in eclipse is plainly $\Delta\phi/\pi$, which attains a maximum of γ/π when the orbit plane contains the sun direction \vec{S}_1 , $\theta_A = 0$.

The pitch and roll and their rates are calculated by the equations of the the previous section.

We may evaluate the effect of excessive roll rate by the inequality

$$|\dot{\rho}| = |\tan p \cos \rho \dot{\phi}|_V \leq 1 \text{ rpm} = 2\pi/60 \text{ rad/sec}$$

and the definitions

$$\dot{\phi}_V = 2\pi/T_V$$

$$T_V = 2\pi \sqrt{\frac{r_v^3}{G M_e}} = 2\pi \sqrt{\frac{r_e^3}{G M_e \sin^3 \gamma}}$$

which reduces to the problem of evaluating the relations between ϕ , θ , γ in

$$\frac{\cos^2 \theta \sin^2 \phi \sin^2 \theta \sin^3 \gamma}{(1 - \cos^2 \theta \sin^2 \phi)^2} \leq \frac{r_e^3}{(60)^2 G M_e}$$

where the right side is a constant. Since for excess roll to occur we must be near $\phi = 0$ (or π), $\theta = 0$ (or π), and the orbital velocity (hence ϕ)

is greatest for low altitude or γ near $\pi/2$, we can approximate the relation for small θ and ϕ by

$$\phi \theta \leq \frac{1}{60} \sqrt{\frac{r_e^3}{G M_e}}$$

Given small θ for the particular orbit (circular, tangent oriented), whenever ϕ_V is within the intervals

$$\Delta \phi \approx \pm \frac{1}{60 \theta} \sqrt{\frac{r_e^3}{G M_e}}$$

on either side of $\phi_V = 0$ or π , we have the excess roll rate condition.

3.6.2 Keplerian Orbit, No Perturbation

Planetary motion in a pure central force field traces out an ellipse with the force center at one focus. Given the initial position and velocity vectors \vec{R}_0 , \vec{V}_0 of an earth satellite, the entire motion is worked out as follows: The angular momentum is conserved; $\vec{R}_0 \times \vec{V}_0 = \vec{L}_0 = \vec{R} \times \vec{V}$ is a constant vector. The energy is conserved, and if a_0 is the semi-major axis and $\mu = G M_e$, we obtain a_0 from the energy equation:

$$\frac{1}{a_0} = \frac{2}{|\vec{R}|} - \frac{|\vec{V}_0|^2}{\mu}$$

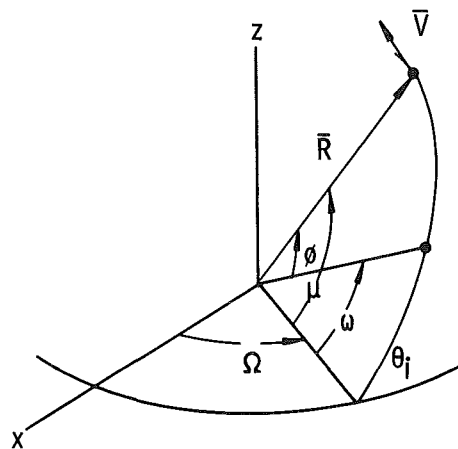
The plane of the orbit contains \vec{R}_0 and \vec{V}_0 , perpendicular to \vec{L}_0 . From \vec{R}_0 and \vec{V}_0 , we are to find the inclination of θ_i of the orbit plane to the (x, y) plane, the orientation ω_0 of the semi-major axis (specifically the perigee direction) in the orbit plane, and the angle Ω_0 between the line of nodes (ascending node) in the (x, y) plane and the x-axis, as well as the angle ϕ_0 from perigee to the present position \vec{R}_0 (Figs. 13 and 14). The order of computing is as follows:

Inclination
$$\theta_i = \frac{\pi}{2} - \sin^{-1} [L_{0z}/|\vec{L}_0|] \quad (0 \leq \theta_{i0} \leq \pi)$$

Longitude of ascending node
(If $\sin \theta_{i0} = 0$, set $\Omega_0 = 0$)
$$\tan \Omega_0 = \{L_{0x}\}/\{-L_{0y}\} \quad (0 \leq \Omega_0 \leq 2\pi)$$

Eccentricity
$$e_0 = \sqrt{1 - \frac{|\vec{L}_0|^2}{\mu a_0}} \quad (0 \leq e_0 \leq 1)$$

Eccentric anomaly
$$E_0 = \frac{\pi}{2} - \sin^{-1} \left[\frac{1}{e_0} \left(1 - \frac{|\vec{R}_0|}{a_0} \right) \right]$$



If $\theta_i = 0$, use $\omega = \Omega + \omega$.

Fig. 13 Orbit Coordinate Angles

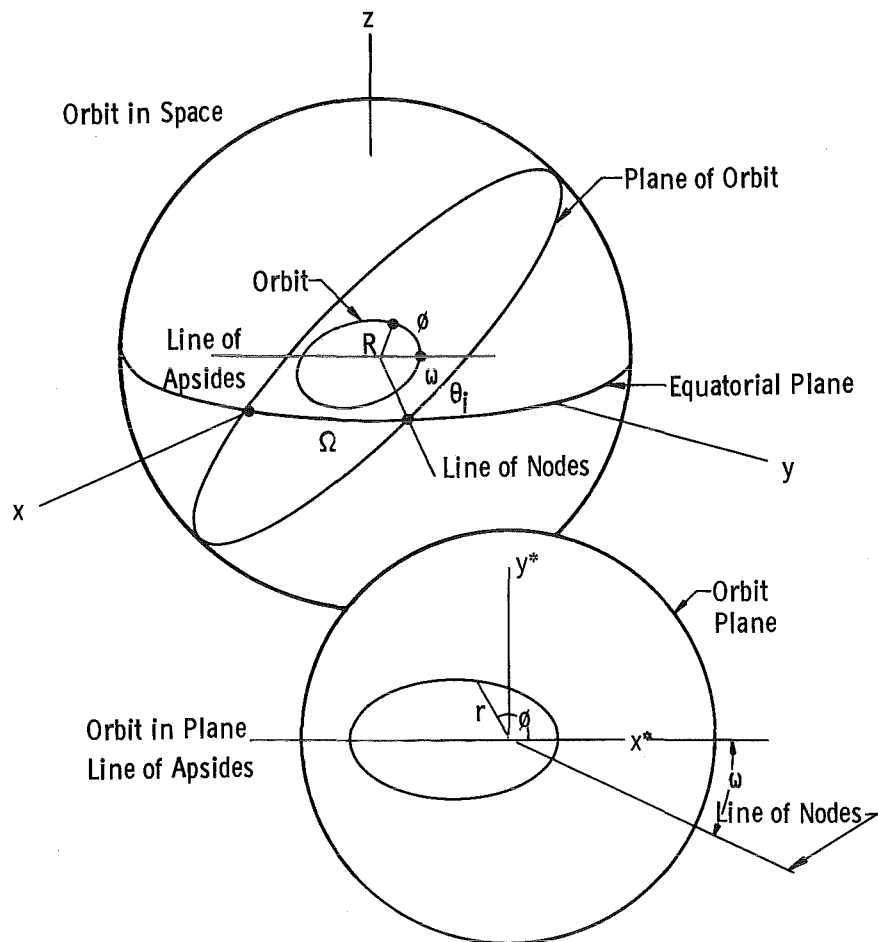


Fig. 14 Orbit in Space and in Plane Illustrating the Euler Angles Ω , θ_i , ω

The sign of $\sin(E_o)$ is the same as the sign of $\vec{R}_o \cdot \vec{V}_o$. If $\vec{R}_o \cdot \vec{V}_o = 0$, then $E_o = 0$; if $|\vec{R}_o| < a_o$, $E_o = \pi$ if $|\vec{R}_o| > a_o$; if $|\vec{R}_o| \equiv a_o$ and $\vec{R}_o \cdot \vec{V}_o \equiv 0$, we may set $E_o = 0$, $e_o = 0$ and circular orbit calculations result. Angle from perigee (true anomaly)

$$\phi_o = \tan^{-1} \left[\frac{\{(1 - e_o^2)^{1/2} \sin E_o\}}{\{\cos E_o - e_o\}} \right]$$

or $\phi_o = 0$ if $e_o = 0$.

Argument of latitude

if $\theta_{io} = 0$

$$\mu_o = \tan^{-1} \left[\frac{\{R_{oz} / \sin \theta_{io}\}}{\{R_{ox} \cos \Omega_o + R_{oy} \sin \Omega_o\}} \right]$$

if $\theta_{io} \neq 0$

$$\mu_o = \tan^{-1} \left[\frac{\{R_{oy}\}}{\{R_{ox}\}} \right]$$

Argument of perigee

$$\omega_o = \mu_o - \phi_o$$

$$\left[\begin{array}{l} \text{Note: The symbol } \tan^{-1} \left[\frac{\{ \}}{\{ \}} \right] \text{ indicates that signs of} \\ \text{both terms are considered to place angle in} \\ \text{proper quadrant.} \end{array} \right]$$

We now have rotation angles Ω_o , θ_{io} , ω_o of an (inverse) Euler rotation from the plane of the ellipse (x^*, y^*) to the (x, y, z) coordinate system. In (x^*, y^*) , we have $x_o^* = r_o \cos \phi_o$, $y_o^* = r_o \sin \phi_o$, $r_o = |\vec{R}_o|$.

In other words, corresponding to the initial \vec{R}_o , \vec{V}_o in (x, y, z) and the definite orbit they prescribe, there exists one ellipse of the same eccentricity and semi-major axis in (x^*, y^*) where the perigee is aligned with the x^* - axis. The angle from ϕ_o is preserved in both spaces, as is angle τ_o between \vec{R}_o , \vec{V}_o .

We will follow the motion in the $(x^* y^*)$ plane, and, through the Euler rotation, recover the corresponding \vec{R} , \vec{V} in the (x, y, z) space. Then at any time, having \vec{R} , \vec{V} , \vec{S} , in (x, y, z) , we may, assuming tangent orientation, compute ϕ_A , θ_A from equations given earlier; hence, roll and pitch. For initial roll and pitch rates, we need $\dot{\phi}_{Ao}$:

$$\dot{\phi}_{Ao} = \dot{\phi}_o + \dot{\tau}_o$$

$$\dot{\tau}_o = \frac{|\vec{L}_o|}{|\vec{R}_o|^2} \left(\frac{\mu}{|\vec{R}_o| |\vec{V}_o|^2} - 1 \right)$$

hence
$$\dot{\phi}_{Ao} = \frac{|\vec{L}_o| \mu}{|\vec{R}_o|^3 |\vec{V}_o|^2} = \frac{\mu \sin^2 \tau_o}{|\vec{R}_o| |\vec{L}_o|}$$

where
$$\tau_o = \frac{\pi}{2} - \sin^{-1} (\vec{R}_{o1} \cdot \vec{V}_{o1})$$

Mean anomaly;

$$M_o = E_o - e_o \sin E_o \quad (\text{Keplers equation})$$

Time since perigee

$$t_{po} = M_o/n_o \quad n_o = \sqrt{\frac{\mu}{a_o^3}} \quad (\text{mean motion})$$

Epoch of perigee passage

$$t_p = t_o - t_{po} \quad (t_o \text{ is initial time of } \vec{R}_o, \vec{V}_o.)$$

To advance the orbit by a time increment T, we advance the time since perigee

$$t = t_{po} + \Delta t = t_o - t_p + \Delta t$$

then

$$M(t) = n_o(t_{po} + \Delta t) = n_o(t)$$

and

$$E(t) - e_o \sin E(t) = M(t)$$

is solved by iteration for E(t).

$$\phi(t) = \tan^{-1} \left[\frac{\{ (1 - e_o^2)^{1/2} \sin E(t) \}}{\{ \cos E(t) - e_o \}} \right]$$

$$r(t) = a_o (1 - e_o \cos \phi(t))$$

$$x^*(t) = r(t) \cos \phi(t)$$

$$y^*(t) = r(t) \sin \phi(t)$$

$$v(t) = \sqrt{\mu \frac{2}{r(t)} - \frac{1}{a_o}}$$

$$\tau(t) = \sin^{-1} \left(\frac{|\vec{L}_o|}{r(t) v(t)} \right) \quad \text{for } \sin \phi(t) > 0$$

$$\tau(t) = \pi - \sin^{-1} \left(\frac{|\vec{L}_o|}{r(t) v(t)} \right) \quad \text{for } \sin \phi(t) < 0$$

$$\tau(t) = \frac{\pi}{2} \quad \text{for } \sin \phi(t) = 0$$

$$v_x^*(t) = v(t) \cos (\phi(t) + \tau(t))$$

$$v_y^*(t) = v(t) \sin (\phi(t) + \tau(t))$$

$$\dot{\phi}_A(t) = \frac{\mu \sin^2 \tau(t)}{r(t) |\vec{L}_o|}$$

We now have new vectors $\vec{R}(t)$, $\vec{V}(t)$ in (x^*, y^*) and can apply the inverse Euler rotation to each using Ω_0 , θ_{i0} , ω_0 to obtain $(\vec{R}(t), \vec{V}(t))$ components in (x, y, z) . From these, as before, we develop roll and pitch values: using ϕ_A , we then obtain their rates.

3.6.3 Keplerian Orbit with Perturbations

All the work of the previous section holds with the exception of the Euler rotation from the orbit plane to the (x, y, z) space. The inclination θ_i of the orbit plane remains unchanged, but the perigee advances or retrogresses, and the plane of the orbit precesses. The earth's oblateness is the cause, through modification of the earth's potential (Fig. 15).

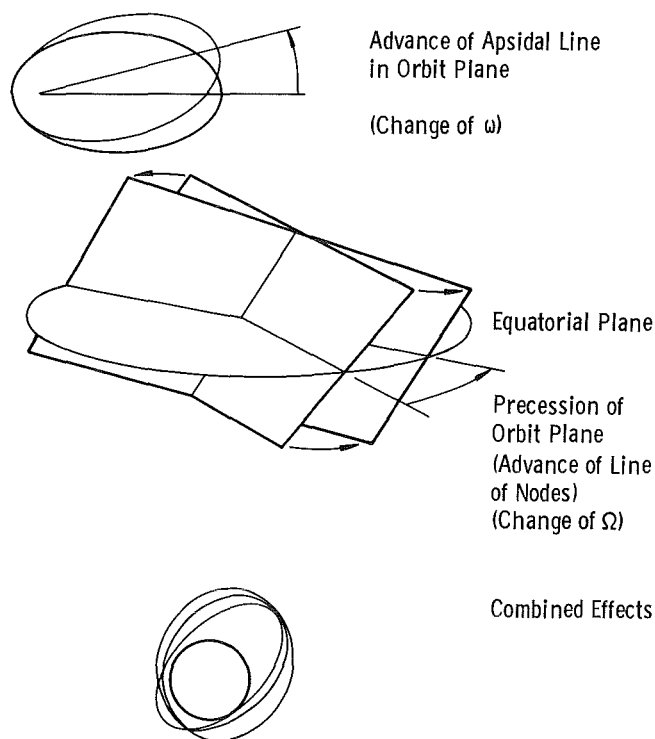


Fig. 15 Secular Perturbations Caused by Earth Oblateness

At any time, with \vec{R} , \vec{V} found in the (x^*, y^*) space, having $B = JR_e^2$, (J is a gravitational potential constant), we calculate

$$\Omega = \Omega_0 - \frac{B (\cos \theta_i) (t - t_0) n_0}{a_0^2 (1 - e^2)^2} \quad \omega = \omega_0 + \frac{B (2 - 2.5 \sin^2 \theta_i) (t - t_0) n_0}{a_0^2 (1 - e^2)^2}$$

n_0 is the mean motion calculated at time t_0 .

ϕ_0 , Ω_0 , and ω_0 are found immediately from \vec{R} , \vec{V} as given before. We assume that e , a , and θ_i are constant, although they are actually oscillatory.

The Euler angles Ω, ω are updated, then the rotation is invoked to generate the \vec{R}, \vec{V} components in (x, y, z) space, and we proceed as before. This process corresponds in part to the Hansen method of computing satellite orbits (Ref. 4).

We believe that this approach to a simulation orbit is novel. It is important since the secular variations may amount to as much as 5 deg per day for near earth satellites (Ref. 5).

3.6.4 "Exact" Orbits

So called exact orbits are obtained as solutions to the differential equations of motion,

$$m_v \ddot{\vec{R}}_v = \Sigma \vec{F} = - \sum_i \frac{G M_v M_i}{(R_{vi})^3} \vec{R}_{vi} + \sum_j \vec{F}_j$$

in which the sum in i is taken over all major bodies concerned with the motion as if each were a simple central force mass (assumed homogeneous, spherical, or point), and the sum in j is over all other forces, whatever their origin, which must be known as, generally, functions of position and time.

A numerical solution is obtained by marching ahead, keeping all force terms up to date, from the initial coordinates and initial time. Several methods are available for this, all requiring fine increments and/or multiple precision arithmetic, all slow to compute. We have found that high precision orbits are costly and may easily require "real time" to compute; hence, they are almost useless for long time scheduling of simulation runs. (These tests were programmed for an IBM 7070). They are however necessary for evaluating any approximate method, such as that of the previous section.

These are two historical numerical methods of solution of the equations of motion. The method of Cowell is quite straightforward, in conjunction with a Runge-Kutta numerical technique. It involves small differences in large numbers and requires multiple precision computer techniques.

The method of Enke is a perturbation method in which the initial conditions establish an osculating ellipse. Small departures from the osculating ellipse are calculated until they grow excessive; then a new osculating ellipse is calculated. The method yields good results without resorting to multiple precision.

For each of these methods, the inclusion of other planetary bodies requires reference to tables of positions, the ephemerides, which are available on copies of the "Themis" tapes (Ref. 3).

Modern methods involve substitution of some faster techniques than the Runge-Kutta procedure in solving the equations. These methods are not self starting but may depend on a Runge-Kutta beginning, after which they require fewer evaluations of the force terms in the differential equations (Ref. 4).

If no velocity dependent forces are involved, the principle secular perturbations are those previously described caused by earth oblateness, all other perturbations being primarily oscillatory. We believe that the method proposed, a single Keplerian osculating ellipse with secular perturbations entering an Euler rotation, is adequate for realistic simulation and is fast to compute.

3.6.5 Arbitrary Flight Paths

It may be required at times to simulate non-periodic motions of vehicles; for example, launch, recovery paths, and transfer orbits. The most general method for this is the direct numerical solution of the differential equations of the motion, for which a complete schedule of thrust magnitude and direction will be required. For approximation purposes, a design trajectory may be adequate with the position vector given as a function of time. From this, the velocity vector is computable. An assumption of vehicle orientation relative to the trajectory allows complete motion description, and when the initial date (accurate to better than the simulation increment, say two minutes) is given, roll and pitch can then be calculated by previous methods.

If we are concerned only with solar radiation, only the coordinates of the vehicle axis (vector A of earlier sections) need be specified. The actual coordinates of position are needed if we are interested in phenomena caused by another body, say earth, such as eclipsing or Albedo illumination.

3.7 SOLAR BANK CONTROL

Only those solar bank modules are to be on which contribute to the illumination of the vehicle. All others are to be off (see section 1.0). Since the vehicle pitches relative to the sun bank, we may consider the projection of the vehicle outline onto the solar bank. Then any solar module entirely outside the outline is to be off, any entirely within shall be on. What about the intermediate cases, partly within, partly without?

We provide three options - a module is inside the outline (on)

1. if any part of it is inside,
2. if its center is inside,
3. if it is entirely inside.

In addition, if the vehicle is in eclipse behind the earth, all modules are off. There will be no intermediate cases for eclipse. An option is provided to either skip the outline calculations or to continue them to show roughly the vehicle outline.

The problem is general as long as the vehicle consists of the following elements:

1. a spherical nose,
2. a cone frustum tangent to the spherical nose, and
3. a right circular cylindrical element of same size as the larger base of the frustum.

Options allow the length of any of these to be zero. Hence most combinations are available with the restrictions that the order be preserved and the sphere diameter be no larger than the cylinder diameter. The body must be everywhere convex.

It is assumed that the vehicle is mounted to rotate about its center of gravity, which is centered in the design centerline of the solar bank, and the vehicle is axially symmetric. Thus the outline of the vehicle projected on the solar bank is single valued in any quadrant and is symmetrical about the vertical centerline on the solar bank.

The program projects the vehicle outline and tests according to the option to determine if the solar module should be on.

The geometry of the vehicle is constant for any run. The pitch angle is variable and is orbit and orientation dependent. The eclipse condition, all solar modules off, is orbit dependent only. Vehicle roll does not enter these calculations because axial symmetry is assumed.

4.0 SECONDARY ILLUMINATION

We have considered in previous sections the means of calculating orbital motion and the main simulation variables, roll and pitch, which properly orient the vehicle to the solar bank. We must now look into the secondary illumination fields, albedo and earth radiance.

Roll of the vehicle takes place within the simulation cell to keep the vehicle "down" direction aimed at earth's center*. Since roll is relative

Move strictly, to keep a particular reference plane, containing the roll axis, aligned with the center of rotation of the body.

to the "birdcage" array, this means that the down direction moves within the birdcage, and this motion is just the roll.

As we will bring out in what follows, the real secondary field has an extended area source, the earth's surface or part of it; hence, the flux arriving at the vehicle in orbit is a continuous function of angle at the vehicle. But the birdcage is a system of six discrete broken line arrays, equally spaced about the vehicle. Thus the best that can be hoped for in simulation is to match integrals of flux. That is, by subdividing the vehicle into six zones, it should be possible to set the six birdcage lines at power levels such that the integrated flux into a zone on the vehicle matches the integrated flux into the same zone on an orbiting vehicle exposed to the real earth illumination source. This is the principle problem of albedo-radiance simulation. Before such matching can be accomplished, it is necessary to know the natures of the real albedo and radiance functions and of the simulation element distribution function.

In our approach to this problem, we assume the vehicle is axially symmetric and tangent oriented. Then we will develop profiles of flux incident on a band around the girth of the vehicle. The profile will depend on position in orbit and the position on the vehicle. So we obtain typically a single profile for each pair of θ_A , ϕ_A values. We then assume that the six birdcage element patterns are of identical form, differing only by equal phase shifts in their arguments and by their amplitudes. The six superimposed birdcage patterns also are shifted relative to the profile by an amount equal to the roll.

The birdcage element illumination pattern at the vehicle depends on the relative size of the birdcage and vehicle and on any optical surfaces involved. This is not known in sufficient detail at this time but will be assumed to have the desirable properties of uniformity over one-sixth the girth of the vehicle with small "tails" extending into neighboring zones.

There is also an axial distribution pattern inherent to the design of heater elements in essentially linear arrangement. If all elements were equally excited along the line, a maximum flux occurs opposite the midpoint of the array. Thus to even out the flux at a fixed distance from the source requires the elements be excited roughly in proportion to the reciprocal of the pattern intensity for a uniformly excited array. The end elements will thus be hotter than the middle elements. This will be treated in detail in section 4.1.

4.1 SECONDARY ILLUMINATION SIMULATION

In this section, we will examine the radiation field produced by an array of linear elements to obtain some idea of the longitudinal distribution of radiation produced by the "birdcage." We confine attention to the cylindrical portion of the array about a cylindrical model. We will assume that the longitudinal and lateral distributions are independent. We look first at the longitudinal distribution.

Now consider an infinitely long line source with flux W emitted per unit length dl (Fig. 16). An element of area dA at distance R is oriented so that it is parallel to the line source and its normal intercepts the line. The flux dW incident on dA is

$$dW = W dA \int_{-\infty}^{+\infty} \frac{\cos^2 \theta}{\rho^2} dl$$

The polar coordinate description of a line is $\rho \cos \theta = R$ and $l = R \tan \theta$, hence,

$$\frac{dW}{dA} = \frac{W}{R} \int_{-\pi/2}^{\pi/2} \cos^2 \theta d\theta = \frac{\pi W}{2R} = I_{\infty}$$

the intensity of flux for an infinitely long line.

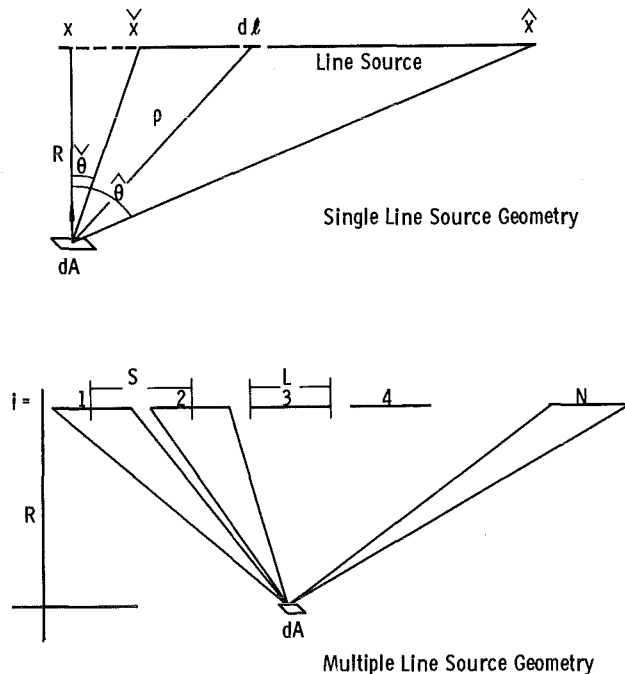


Fig. 16 Geometry for Study of Longitudinal Flux Distributions

For a finite line, the previous integral is evaluated between finite limits:

$$\frac{W}{R} \int_{\theta_v}^{\theta_A} \cos^2 \theta d\theta = I_F$$

And for an array of N linear line segments ($i = 1, 2, \dots, N$), we have

$$\frac{W}{R} \sum_{i=1}^N \int_{\theta_i^v}^{\theta_i^A} \cos^2 \theta d\theta = I_{F,N}$$

The limits of integration θ_i^v, θ_i^A are determined by the location of the area element dA relative to the ends of the i^{th} element. It is convenient to normalize relative to the infinite line flux I_∞ . Then the integrals are of form

$$\frac{I_{F,i}}{I_\infty} = \frac{1}{\pi} \left[\tan^{-1} \left(\frac{x_A - x}{R} \right) + \frac{x_A - x}{(x_A - x)^2 + 1} \right]_{x=x_i^v}^{x=x_i^A}$$

If N elements, each of length L, spaced S on centers, are considered, we obtain

$$\frac{I_{F,N}}{I_\infty} = \frac{1}{\pi} \left[\sum_{i=1}^N \tan^{-1} \frac{R L}{R^2 + (\hat{x}_i - x)(\hat{x}_i - x)} + \frac{R(\hat{x}_i - x)}{R^2 + (\hat{x}_i - x)^2} - \frac{R(\hat{x}_i - x)}{R^2 + (\hat{x}_i - x)^2} \right]$$

where $\hat{x}_i = \hat{x}_i + L, \hat{x}_{i+1} = \hat{x}_i + S.$

The results for various values of R are plotted in Fig. 17 for ten elements having $L = 0.9, S = 1$. For comparison, the results for $R = 10, L = 10, S = 10$ are plotted, showing that at a little distance, the small discontinuities in an interrupted line source are washed out, and the flux is essentially that of a single source of slightly less strength of the same overall length. (See Ref. 6 for results of additional work at AEDC on the line source arrays.)

The important feature here is the gross shape of the curves, maximum at center and dropping at ends. This means that the inverse of this function, or of its piecewise integrals, will be needed to weight the intensities of the individual elements of the source to provide a uniform illumination region at R distance from the source.

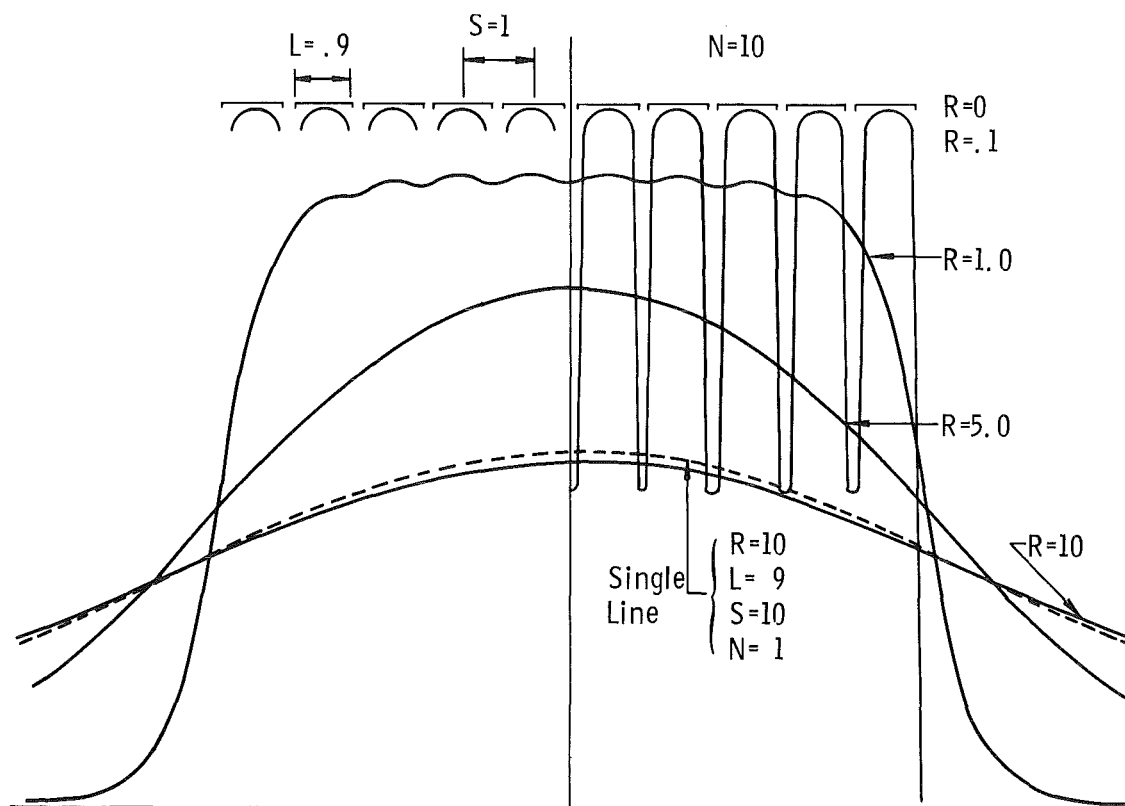


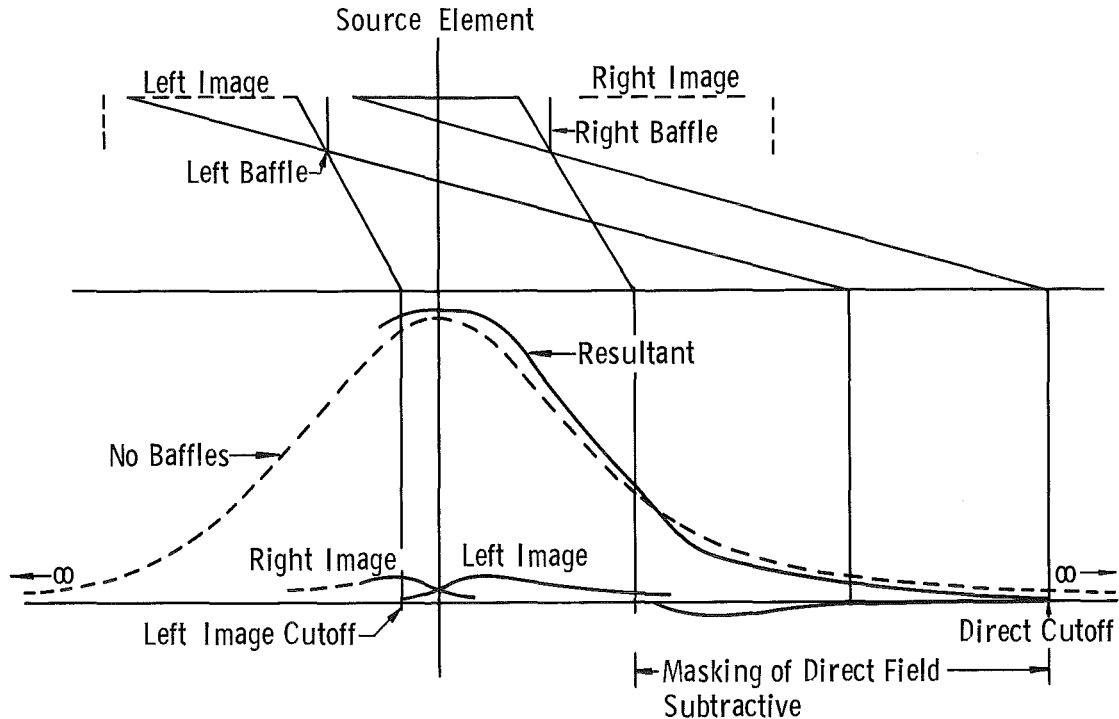
Fig. 17 Longitudinal Flux Distribution for Line Source Arrays as Function of Distance from Line

Now the actual birdcage elements are not simple linear sources; they are rods of definite size at the foci of cylindrical reflections of roughly piecewise parabolic segment cross section. The reflector design is aimed at defining rather sharply the lateral illumination on a specific body (nominally a right circular cylinder plus cone). The reflectors thus have the principle characteristic of cylinder optical elements; they are astigmatic. This means that any point in object space (on the source element) will be imaged (real or virtual) as a line in image space. This fact adds to the validity of the foregoing discussion.

The real line source elements are separated by plane baffles perpendicular to the line, perhaps reflectors, to limit the angular extent of radiation. Since their dimensions are small relative to the length of line segment, they effect the distribution only slightly, probably insignificantly. They most strongly influence the flux arriving at a given point from most remote elements, which contribute very little in any case.

The result of baffling is indicated in Fig. 18 for a single element. The main features are slight increase and flattening of peak, an addition

to shoulder, a reduction of heel, and a finite termination of the tail of the distribution, all minor. The N element distribution can be obtained by superposition.



Limited to Single Reflections by Perfect Mirrors; Subsequent Reflections Contribute Much Less.

Fig. 18 Approximate Effect of Reflecting End Baffles on Longitudinal Flux Distribution for a Single Line Source Element

The source elements are in reality small rods rather than lines. We have used the notation W for intensity per unit length from a line. For a directionally homogeneous radiating line, whatever radiation leaves the line also passes through a cylinder of sufficiently small diameter concentric with the line. If the rod dimensions are small relative to other lengths, the assumption of ideal line source is a good approximation.

We have assumed that the lateral and longitudinal distributions are independent. This is an essential point with respect to computability. If it is necessary to control all elements of the birdcage independently, we shall have to solve frequently a set of 192 equations in 192 unknowns to find the amplitudes at which to excite the 192 birdcage elements. If the assumed independence is valid, this reduces to 6 equations in 6 unknowns for the lateral distribution and to the application of a previously evaluated weighting function for the longitudinal distribution.

We must mention some design problems posed by the birdcage array. First, a vehicle's base will intercept secondary illumination, but base illumination does not occur in the birdcage design, except incidentally.

Second, a real vehicle of say cylinder-cone configuration, when about horizontal, will have a zone "on top" the cylinder which cannot see the earth; whether the top of the cone has such a zone depends on the altitude and cone angle. If the half cone angle is greater than the horizon depression with altitude, the cone will be illuminated when the cylinder is not. But the birdcage elements will not discriminate; if an element is "on" to illuminate the cone it will also illuminate the neighboring cylinder which should not be illuminated. If the vehicle nose is ogival or another smoothly faired shape having no discontinuity of slope where it joins the cylinder body, this is not so severe a problem.

Third, the sharpest defined boundary for illumination with line sources and cylindrical reflectors are the lateral boundaries, parallel to line arrays. All other boundaries are smeared by the astigmatic reflectors. Thus it is not possible to sharply define the illumination on a pointed nose piece. A practical solution here would be to define the nose by means of a cone frustrum roughly matching the nose shape. The nose illumination pattern will be inefficient in any case, and considerable illumination will pass directly to the test chamber walls and increase the heat load.

4.2 "BIRDCAGE" PATTERNS AND MATCHING

Assuming that we know the combined illumination profile on a vehicle in orbit, we must go through some computations to find the birdcage excitation required to effectively reproduce this profile on the test vehicle (Figs. 19, 20, 21, and 22).

If there are M discrete sources of amplitudes a_i ($i = 1, 2, \dots, M$), having distribution functions g_{ik} (from source i into region k on vehicle) and the profile function f_k (from real source into region k), the best we can hope to do is to match the total input into each of the M regions, by proper selection of a_i , matching real input to simulating input over each region k . We are limited to M regions on the vehicle by the M discrete sources, assumed so arranged as to cover the vehicle.

We require for the area S_k of each k region, $k = 1, 2, \dots, M$,

$$\int_{S_k} f_k dS = \sum_{i=1}^M a_i \int_{S_k} g_{ik} dS$$

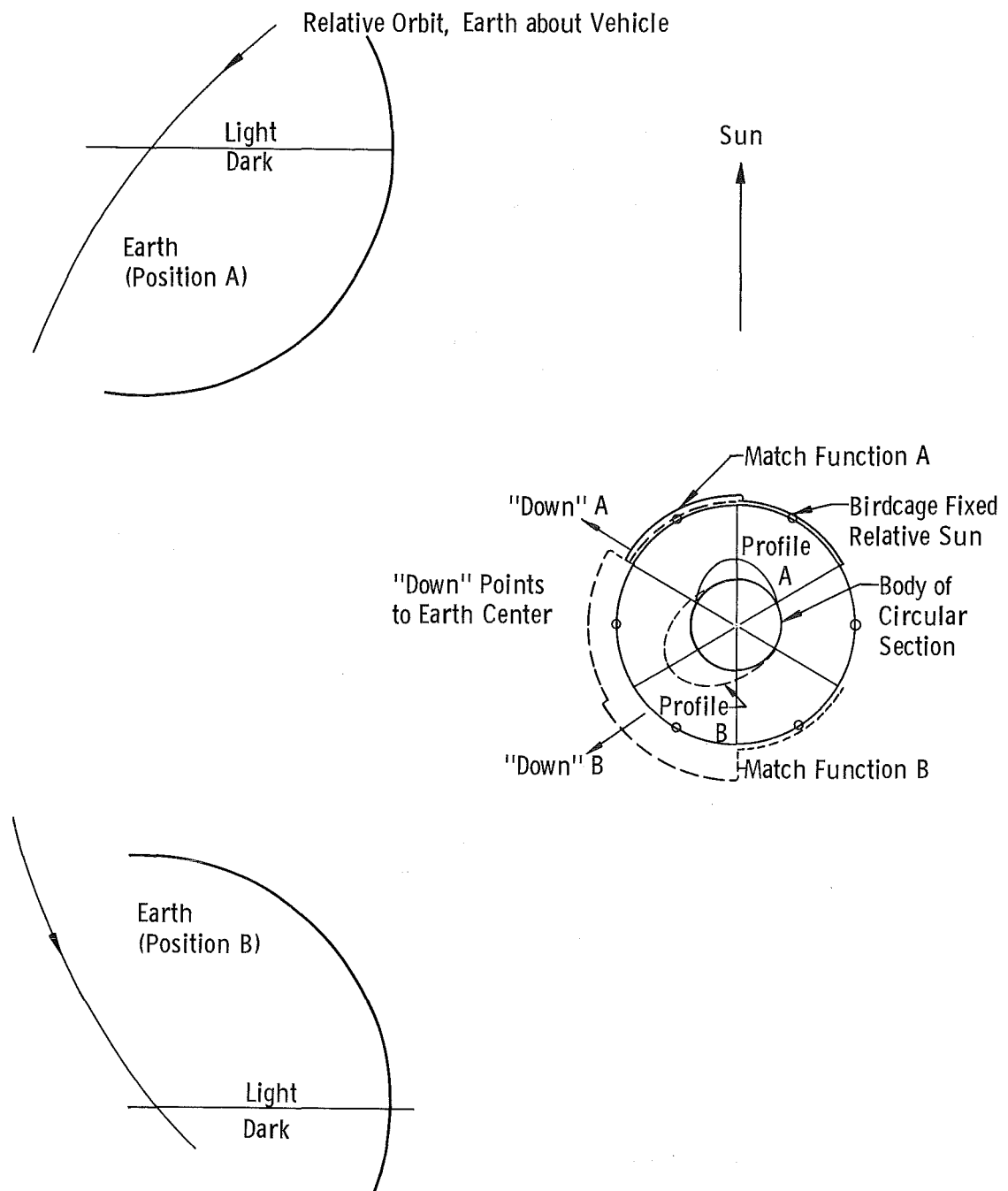


Fig. 19 Integral Profile Matching

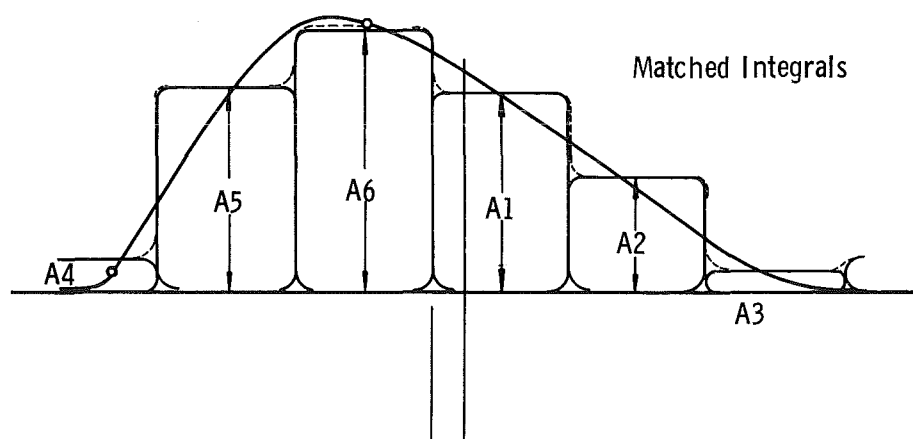
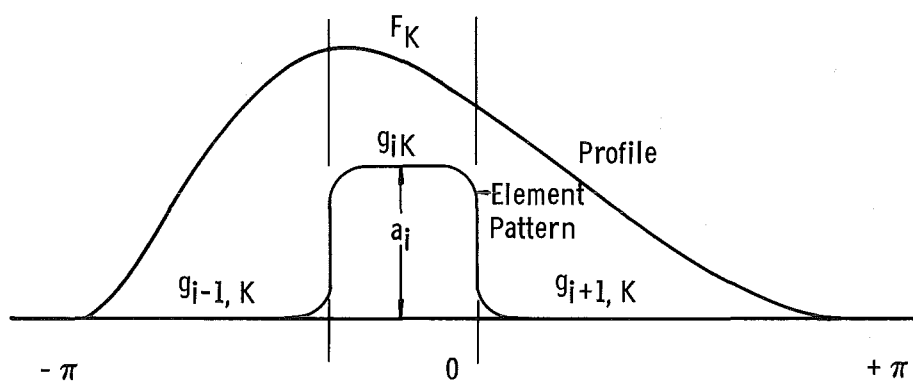


Fig. 20 Profile Matching with Integrals

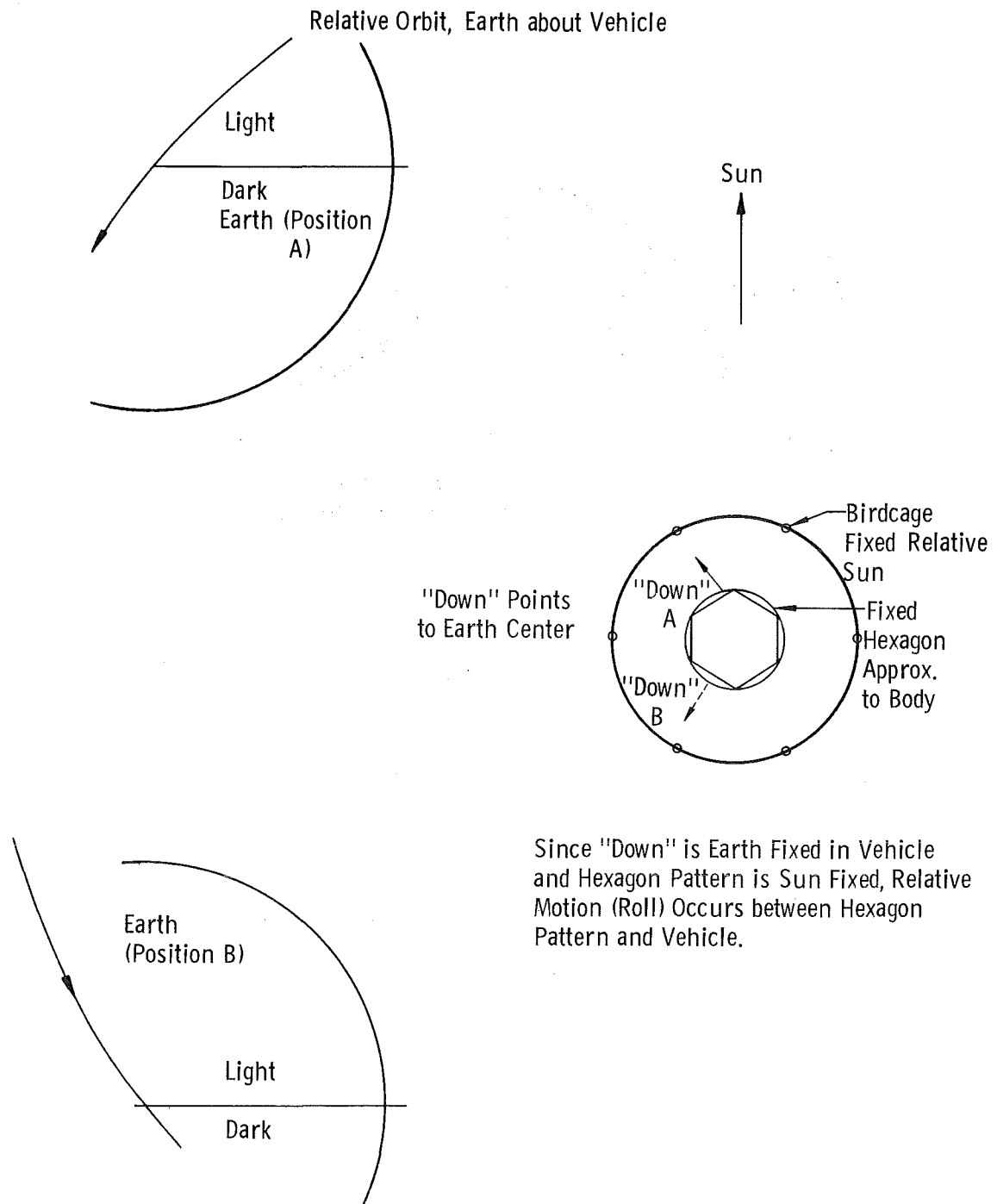


Fig. 21 Six-Point Profile Matching

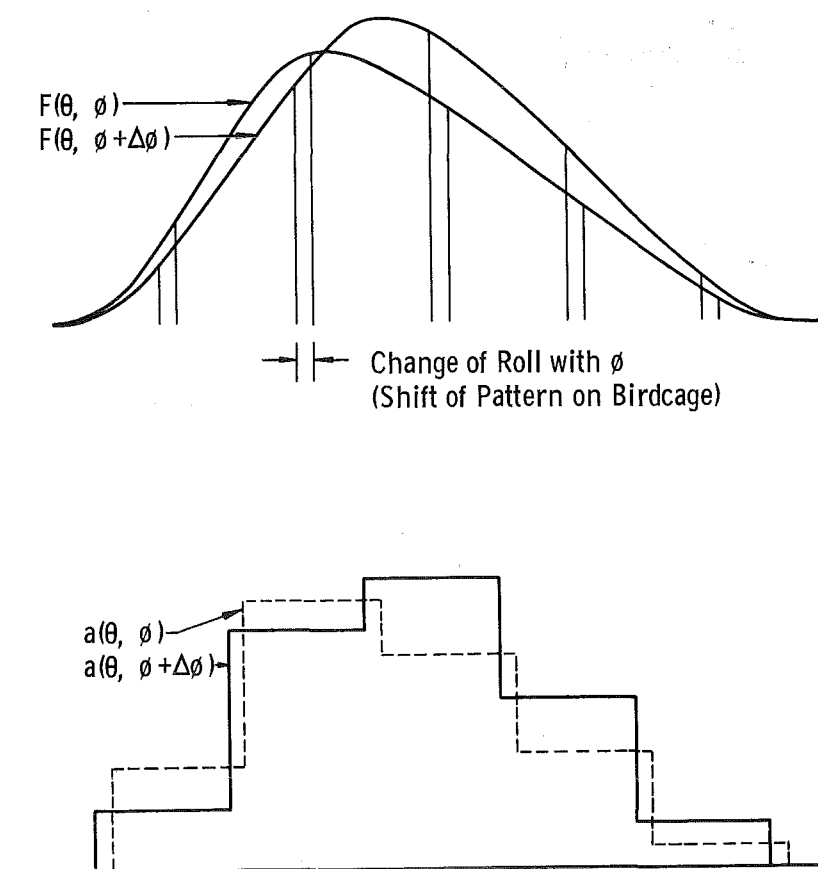


Fig. 22 Profile Matching at Six Points Only

The g_{ik} are fixed by birdcage element-reflector geometry. The f_k are orbit-orientation functions and depend on position on the vehicle. They depend on location on the vehicle surface and on the time, through orbit position. We require a set of a_i for each simulation interval (nominally two minutes real time).

The direct solution of this system of M equations in M unknowns leads to appearance of negative a_i 's, obviously meaningless. By a "least squares" approach, we obtain the system of normal equations

$$\sum_{i=1}^M a_i \sum_{k=1}^M G_{ik} G_{jk} = \sum_{k=1}^M F_k G_{jk} \quad , j = 1, 2, \dots, M$$

where we have used the definitions

$$G_{ij} = \int_{S_k} g_{ij} dS \quad F_k = \int_{S_k} f_k dS$$

In vector-matrix notation, we have

$$\{S\} \vec{a} = \vec{V} \quad \text{or} \quad \vec{a} = \{S\}^{-1} \vec{V}$$

where $\{S\}$ is a matrix of elements

$$S_{ij} = \sum_k G_{ij} G_{ik}$$

$$\{S\}^{-1} \text{ is its inverse}$$

$$\vec{V} \text{ is a vector of components } V_j = \sum_k F_k G_{jk}$$

$$\vec{a} \text{ is a vector of components } a_i$$

Ordinarily the matrix elements are functions of geometry and orientation of the vehicle-discrete-source system, and the V_j are functions of vehicle position, orientation, altitude, etc., as well. We may say the V_j are orbit dependent (through the f_k function) and roll dependent (through the g_{ik} function) since they depend on roll of vehicle within the birdcage.

But if the vehicle is perfectly axially symmetric in shape and surface properties, the g_{ik} become independent of roll; hence, the matrices $\{S\}$ and $\{S\}^{-1}$ have constant elements, and the V_j are independent of roll. This point is of considerable significance.

If the S matrix is constant, we may immediately invert it one time for $\{S\}^{-1}$ and program the evaluation of M equations in M unknowns at each point in orbit. But if the $\{S\}$ matrix is variable, we must invert it for $\{S\}^{-1}$ at each point in orbit, then solve the M equations in M unknowns.

For the most rapid computing, if the resulting errors are not excessive in practice, we may replace the circular section, on which the profiles are based, by a hexagonal section. Each leg of the hexagon directly faces one of the birdcage line elements, and we ignore any "tails" of the element distribution function. Then the amplitudes a_i are directly associated with six corresponding points on the profile.

Since the profile pattern changes continually with orbit position, and roll changes similarly, we must still evaluate six new profile amplitudes at each point in orbit. These are unique calculations at each point in realistic orbits and repeat periodically only for a static universe orbit model in which the orbit period is an exact multiple of the simulation interval (2 min).

4.3 ILLUMINATION INTEGRALS

To compute earth Albedo and radiance integrals for a surface element having arbitrary orientation and position, we make the following assumptions:

1. that Albedo is a uniform property of earth's surface,
2. that the earth is a sphere,
3. that the earth's surface is diffusely reflecting, and
4. that the earth has no atmosphere.

I_S Solar constant, intensity of solar radiation at earth

a_e Albedo, fraction of solar constant reflected, a surface property

The solar radiation incident on an area element ΔA_1 having its normal inclined at angle θ_e to sun direction I_S

$$\Delta I_e = \begin{cases} I_S \cos \theta_e \Delta A_1 & \text{for } \cos \theta_e \geq 0 \\ 0 & \text{for } \cos \theta_e < 0 \end{cases}$$

Of this a fraction a_e is reflected diffusely by ΔA_1 ; hence, the intensity per unit solid angle ΔI_ψ in a direction inclined at angle ψ to the surface normal is

$$\Delta I_\psi = \frac{a_e I_S}{\pi} \cos \theta_e \cos \psi \Delta A_1$$

The intensity included in solid angle $\Delta \omega$ is

$$\Delta I_\omega = \frac{a_e I_S}{\pi} \cos \theta_e \cos \psi \Delta A_1 \Delta \omega$$

An area element ΔA_2 , at distance ρ_e from ΔA_1 , having its normal inclined at angle ξ to the direction of ρ_e , intercepts a solid angle (Fig. 23).

$$\Delta \omega = \frac{\Delta A_2 \cos \xi}{\rho_e^2}$$

Hence the intensity arriving at ΔA_2 is

$$\Delta I_2 = \frac{a_e I_S}{\pi \rho_e^2} \cos \theta_e \cos \psi \cos \xi \Delta A_1 \Delta A_2$$

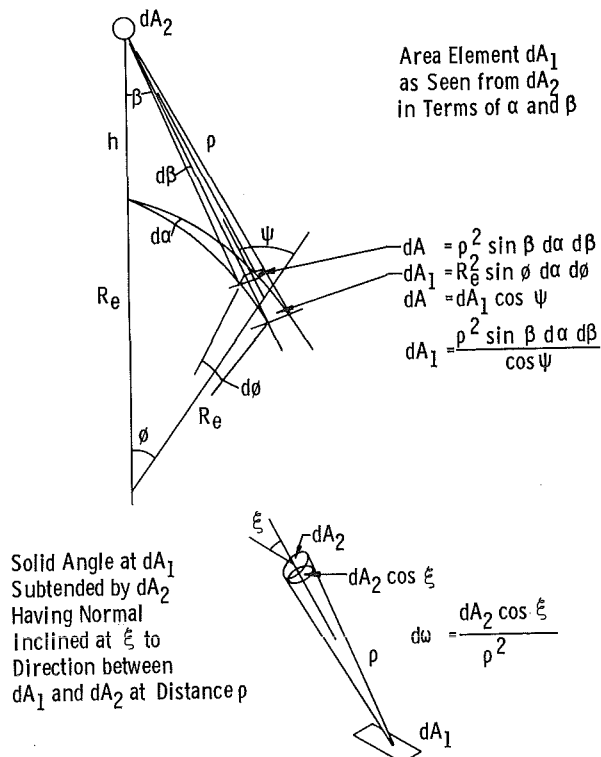


Fig. 23 Solid Angle Geometry for Albedo and Earth Radiance Calculation

Let the area element ΔA_2 be located at altitude h above earth of radius R_e (Fig. 24). From this point, the portion of the earth that can be seen is confined within a horizon circle. The angle γ between the direction of earth center and the horizon circle is defined by

$$\sin \gamma = R_e / (R_e + h) \quad (0 < \gamma < \frac{\pi}{2})$$

At the earth center, let θ_s be the angle between the direction to ΔA_2 and the sun direction; let θ_e be the angle between the area element ΔA_1 on earth and the sun; let ϕ_e be the angle between the directions of ΔA_1 and ΔA_2 .

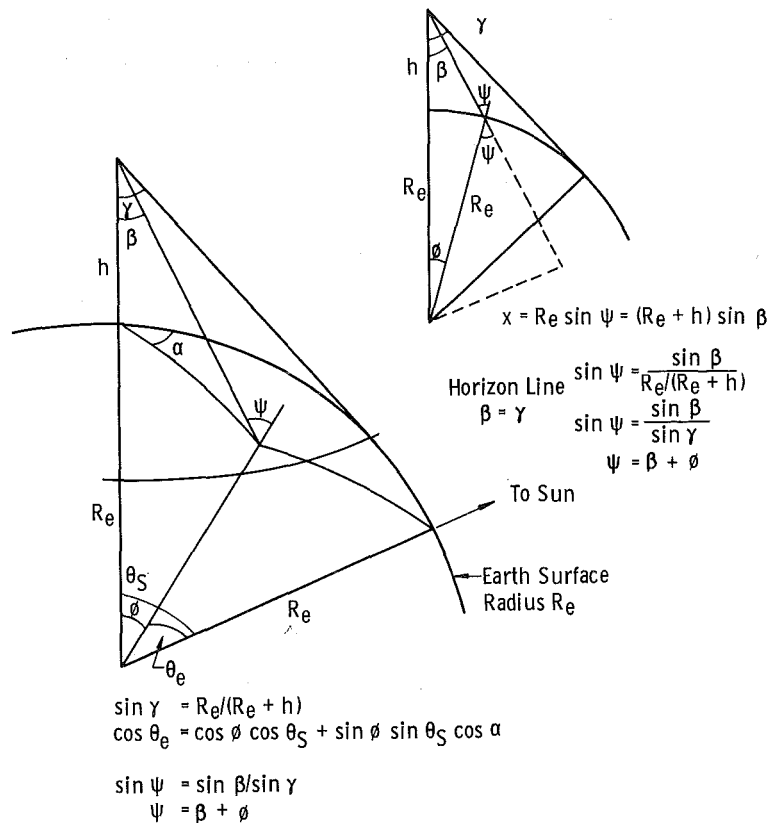


Fig. 24 Coordinate Relations for Albedo and Earth Radiance Calculation

At the element ΔA_2 , ψ is the angle between the normal to A_1 and the direction of ΔA_2 , as before.

At the element Δ_2 , let β be the angle between the direction to earth center and Δ_1 . Angle β is a "nadir" angle.

Then the following relations hold:

$$\psi = \beta + \phi$$

$$\sin \psi = \sin \beta / \sin \gamma$$

$$\cos \theta_e = \cos \theta_S \cos \phi_e + \sin \theta_S \sin \phi_e \cos \alpha$$

where α is the angle about the line from ΔA_2 to earth center measured from the plane including this line and the sun. Angle α is the azimuth angle (Fig. 25).

Now the element $\Delta\mathbf{A}_1$ is described in spherical coordinates having polar axis along the earth-to- $\Delta\mathbf{A}_2$ line, longitude α , and co-latitude ϕ_e :

$$\Delta A_1 = R_e^2 \sin \phi_e \, d\alpha \, d\phi_e$$

Integrating over the interior of the horizon circle, we obtain

$$\frac{I_2}{\Delta A_2} (\Delta A_2, \theta_S, \gamma, \xi) = \frac{a_e I_S}{\pi} \int_{\beta=0}^{\gamma} \int_{\alpha_{\min}}^{\alpha_{\max}} \cos \theta_e (d, \beta, \theta_S, \gamma) \cos \xi \sin \beta \, d\beta \, d\alpha$$

where α_{\min} , α_{\max} may be functions of β , and there may be several distinct regions or functions.

In the spherical coordinates α , β , any orientation of surface element may be described by the direction angles of its normal, α_N , β_N (Fig. 26). Then the angle ξ is found from

$$\cos \xi = \cos \beta \cos \beta_N + \sin \beta \sin \beta_N \cos (\alpha - \alpha_N)$$

Since

$$\theta = \psi - \beta, \quad \text{and} \quad \sin \psi = \sin \beta / \sin \gamma$$

$$\begin{aligned} \cos \theta_e &= \sin \psi (\cos \theta_S \sin \beta + \sin \theta_S \cos \beta \cos \alpha) \\ &\quad + \cos \psi (\cos \theta_S \cos \beta - \sin \theta_S \sin \beta \cos \alpha) \end{aligned}$$

The intensity integrand is completely expressible in the two variables α , β , and the configuration parameters θ_S , γ , α_N , β_N .

At this stage it is possible to integrate numerically by letting α range from 0 to 2π and β range from 0 to γ , provided that

$$\cos \xi \geq 0$$

$$\cos \theta_e \geq 0$$

$$\cos \psi \geq 0$$

and using ($=0$) for any (α, β) violating these conditions. This will be discussed later in Appendix IV.

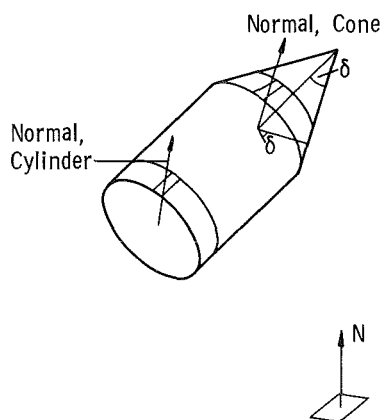


Fig. 26 Area Elements for Cylinder-Cone

Ignoring for the moment the constant $a_e I_S/\pi$, we have the following terms to be integrated over α and β :

1. $\cos \beta_N \cos \theta_S \cos^2 \beta \sin \beta \cos \psi$
2. $-\cos \beta_N \sin \theta_S \cos \beta \sin^2 \beta \cos \psi \cos \alpha$
3. $\cos \beta_N \cos \theta_S \cos \beta \sin^2 \beta \sin \psi$
4. $\cos \beta_N \sin \theta_S \cos^2 \beta \sin \beta \sin \psi \cos \alpha$
5. $\sin \beta_N \cos \theta_S \cos \alpha_N \sin^2 \beta \cos \beta \cos \psi \cos \alpha$
6. $\sin \beta_N \cos \theta_S \sin \alpha_N \sin^2 \beta \cos \beta \cos \psi \sin \alpha$
7. $-\sin \beta_N \sin \theta_S \cos \alpha_N \sin^3 \beta \cos \psi \cos^2 \alpha$
8. $-\sin \beta_N \sin \theta_S \sin \alpha_N \sin^3 \beta \cos \psi \sin \alpha \cos \alpha$
9. $\sin \beta_N \cos \theta_S \cos \alpha_N \sin^3 \beta \sin \psi \cos \alpha$
10. $\sin \beta_N \cos \theta_S \sin \alpha_N \sin^3 \beta \sin \psi \sin \alpha$
11. $\sin \beta_N \sin \theta_S \cos \alpha_N \sin^2 \beta \cos \beta \sin \psi \cos^2 \alpha$
12. $\sin \beta_N \sin \theta_S \sin \alpha_N \sin^2 \beta \cos \beta \sin \psi \sin \alpha \cos \alpha$

Note: $\sin \psi = \sin \beta / \sin \gamma$

As long as there are no boundaries of earth surface for which $\alpha = \alpha(\beta)$, so that α can range from 0 to 2π , we may integrate relative to α and obtain simple results. Integrals (1, 3) do not contain α so the integration results in a factor 2π . Integrals (2, 4, 5, 6, 9, 10) contain only $\sin \alpha$ or $\cos \alpha$ and vanish. Integrals (7, 8, 11, 12) contain $\cos^2 \alpha$ or $\cos \alpha \sin \alpha$ and result in a factor of π .

These conditions are satisfied as long as we have both

$$\beta_N \leq \frac{\pi}{2} - \gamma$$

$$\theta_S \leq \gamma$$

If $\beta_N \geq \pi/2 + \gamma$ or $\theta_S \geq \pi - \gamma$, the earlier conditions on $\cos \xi$ or $\cos \theta_e$ are violated and the entire integral ($I_2/\Delta A_2$) vanishes.

For $\frac{\pi}{2} - \gamma < \beta_N < \frac{\pi}{2} + \gamma$

and/or $\gamma < \theta_S < \pi - \gamma$

there exist boundaries of form $\alpha(\beta)$, and the integration becomes complicated. The integration is bounded by arcs of one, two, or three curves of $\alpha(\beta)$, whose intersections are generally given by implicit functions. A first integration may be done formally; expressions result for which the integrals are not available in closed form.

Numerical integration may be accomplished in an easily comprehended manner by referring to the earlier integral expression. The product $\cos \xi \cos \theta_e \sin \beta$ may be calculated term by term, and in addition, the expression $\cos \psi$ can be evaluated to ensure that the conditions

$$\left. \begin{array}{l} \cos \xi \\ \cos \theta_e \\ \cos \psi \end{array} \right\} \geq 0$$

are satisfied.

For some value combinations of $\alpha_N, \beta_N, \theta_S$ the integrations can be carried out. Five special cases are given in Appendix II. A typical body for which profiles are easily obtained, assuming circular orbit, tangent orientation, is shown in Fig. 26.

4.4 RADIANCE FUNCTIONS

4.4.1 Earth Radiance Integrals

The earth is taken to be a warm body, uniform, having a flux I_r issuing from each element of area. The corresponding flux arriving at the element of area ΔA_2 is obtainable from the albedo integral by setting $\cos \theta_e = 1$ and replacing constant I_s by I_r .

$$\frac{I_2}{\Delta A_2} = \frac{I_r}{\pi} \int_{\alpha} \int_{\beta} \cos \xi \sin \beta \, d\beta \, d\alpha$$

and $\cos \xi = \cos \beta \cos \beta_N + \sin \beta \sin \beta_N \cos (\alpha - \alpha_N)$, as before.

The integration is given in Appendix III with changes in form depending on the boundary relationships. The closed forms are available because of the great simplification of integration over a region bounded by one or two arcs and the simpler integrand.

4.4.2 Combined Secondary Illumination

The illumination intensity to be simulated by the birdcage is the combined Albedo-earth radiance functions

$$\begin{aligned} \frac{I\beta}{\Delta A_2} &= \frac{I_s a_e}{\pi} \int \int \cos \theta_e \cos \xi \sin \beta \, d\beta \, d\alpha \\ &+ \frac{I_r E_{FF}}{\pi} \int \int \cos \xi \sin \beta \, d\beta \, d\alpha \end{aligned}$$

A factor (E_{FF}) is included in the second term for purposes of correcting the spectral differences between earth and the incandescent heater elements of the birdcage. This factor may be in fact a function of position on the vehicle, hence a function of the roll angle. It is a surface property of the vehicle.

5.0 CONCLUSIONS

Provided that some simplifications are allowed, it is possible to organize a digital computer system of 7074 programs which will provide realistic orbit calculations and control of all the Mark I simulation parameters in a small fraction of real time. Any violation of the simplifying assumptions will require some special programming and generally more computer time. Most of the program types have been written and run in connection with Mark I projects but only piecemeal. A logical, next step in this sequence is the organization of a comprehensive program to do all required calculation for really typical test vehicle-orbit configurations with as high realism as computer-time-to-real-time ratios will allow. Perhaps a more immediately practical approach would be to develop a fast computing program system using rather gross approximations and to develop a slower, more accurate, highly realistic study system for evaluating the overall results of approximations on the quality of Mark I performance and test results. Having then the two extremes programs available, future efforts would be aimed at obtaining an efficient practical compromise.

REFERENCES

1. Cunningham, Fred G. "Calculations of the Eclipse Factor for Elliptical Satellite Orbits." NASA-TN-D-1347, June 1962.
2. The American Ephemeris and Nautical Almanac for the Year 1963. United States Government Printing Office, Washington, 1961.
3. "Themis Code" Tapes produced by the University of California Radiation Laboratory for the Wright Air Development Center, Air Force Systems Command.
4. Phelan, Howard T. "Computation of Satellite Orbits by the Hansen Method as Modified by Musen." NASA-TR-R-147, 1962.
5. Sterne, Theodore E. An Introduction to Celestial Mechanics. Interscience Publishers, 1960.

6. Mulkey, M. R., Klautsch, R. E., Rayfield, G. A., and Sherrell, F. G. "Space Simulation Chamber Instrumentation." AEDC-TDR-63-113, June 1963.
7. Jaatinen, W. A., Rothacker, D. L., Bull, R. H., Dachs, M. A., and Shenker, M. R. "Solar Radiation Simulation Studies, Part I." AEDC-TDR-63-90, May 1963.
8. Jaatinen, W. A., Rothacker, D. E., et al. "Solar Radiation Simulation Studies, Part II." AEDC-TDR-63-91, May 1963.
9. Fitz, C. D., Lukasik, S. J., et al. "Albedo and Planet Radiation Intercepted by an Earth Satellite." AEDC-TDR-63-92, May 1963.

APPENDIX I

A LIST OF IBM 7074 PROGRAMS CONCERNED WITH MARK I ILLUMINATION SIMULATION

Program No.	Title
05027	Interplanetary Trajectory Study Mark I
05028	Orbit Calculations
05032	Interplanetary, Trajectory Study Mark I (RSW-1)
05036	Double Precision Orbits
05036	Orbit Subroutine
05045	Encke Orbit
05048	Interplanetary Trajectory (RSW-2)
05049	Interplanetary Trajectory (RSW-3)
05050	Orbit III
05051	Radiation Study
05064	Albedo Ray Trace (1)
05073	Albedo Profiles
05087	Total Heat Input, Cone or Cylinder
05090	Themis Translation
05092	Roll Pitch Plot
05109	Albedo Plot
05122	Albedo Profile Transformation
05123	Albedo Integration
05133	Albedo Integral, Transition
05205	Solar Simulation Module Honeycomb
05064	Albedo Ray Trace
05212	Albedo Ray Trace Revision
05216	Albedo Mirror Design

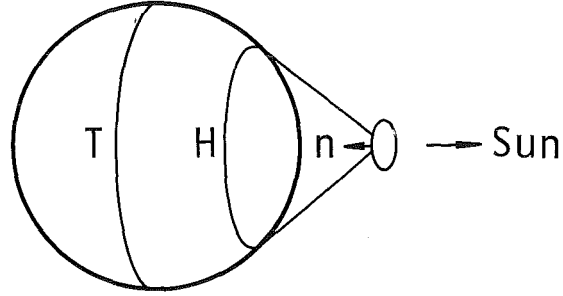
APPENDIX II

SPECIAL CASES OF ALBEDO INTEGRAL

CASE 1

ΔA_2 horizontal ($\beta_N = 0$) and located on line between earth and sun ($\theta_S = 0$).

This gives the maximum value of the integral and is very useful for order of magnitude estimates. With $\beta_N = 0$, $\theta_S = 0$, integrands (1, 3) are the only contributors:



$$1(a) \quad 2\pi \cos \beta_N \cos \theta_S \cos^2 \beta \sin \beta \cos \psi \, d\beta$$

$$3(a) \quad \cos \beta_N \cos \theta_S \cos \beta \sin^2 \beta \sin \psi \, d\beta$$

become

$$1(b) \quad 2\pi \cos^2 \beta \sin \beta \sqrt{1 - \frac{\sin^2 \beta}{\sin^2 \gamma}} \, d\beta$$

$$3(b) \quad 2\pi \cos \beta \frac{\sin^3 \beta}{\sin \gamma} \, d\beta$$

which are simply transformed to

$$1(c) \quad 2\pi \frac{\cos^2 \beta}{\sin \gamma} \sqrt{\cos^2 \beta - \cos^2 \gamma} \, d(-\cos \beta)$$

$$3(c) \quad 2\pi \frac{\sin^3 \beta}{\sin \gamma} \, d \sin \beta$$

3(c) integrates simply to $\frac{\pi}{2} \sin^3 \gamma$ over the β range $(0, \gamma)$ while 1(c) integrates to

$$\frac{\pi}{2} \left\{ \sin^3 \gamma + \frac{\cos^2 \gamma \sin \gamma}{2} + \frac{\cos^4 \gamma}{2} \ln \left(\frac{\cos \gamma}{1 + \sin \gamma} \right) \right\}$$

So for the "hot spot" ($\beta = 0$, $\theta_S = 0$)

$$\frac{I_2}{\Delta A_2} = a_e I_S \left[\sin^3 \gamma + \frac{\cos^2 \gamma}{4} \left\{ \sin \gamma + \cos^2 \gamma \ln \left(\frac{\cos \gamma}{1 + \sin \gamma} \right) \right\} \right]$$

CASE II

ΔA_2 is located over the terminator ($\theta_S = \pi/2$) and horizontal. Integrands (2, 4) survive. The range of α is $(-\pi/2, +\pi/2)$.

$$2. \quad -\cos \beta \sin^2 \beta \cos \psi \cos \alpha \, d\alpha \, d\beta$$

$$4. \quad \cos^2 \sin \beta \sin \psi \cos \alpha \, d\alpha \, d\beta$$

$$\begin{aligned} 2(a) \quad & -\cos \beta \sin^2 \beta \sqrt{1 - \frac{\sin^2 \beta}{\sin^2 \gamma}} \, d(\sin \alpha) \, d\beta \\ & = -\sin^2 \beta \sqrt{1 - \frac{\sin^2 \beta}{\sin^2 \gamma}} \, d(\sin \alpha) \, d(\sin \beta) \end{aligned}$$

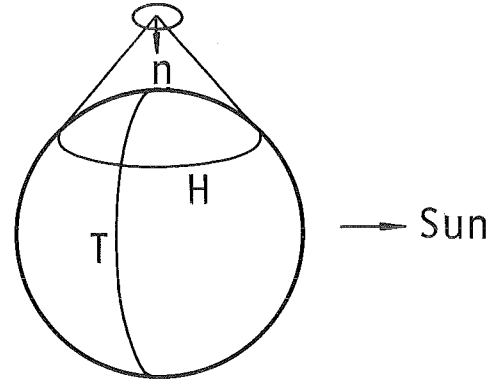
integrating to

$$\begin{aligned} 2(b) \quad & -\frac{2}{\sin \gamma} \left[-\sin \beta (\sin^2 \gamma - \sin^2 \beta)^{3/2} + \frac{\sin^2 \gamma}{8} \left\{ \sin \beta (\sin^2 \gamma - \sin^2 \beta)^{1/2} \right. \right. \\ & \left. \left. + \sin^2 \gamma \sin^{-1} \left(\frac{\sin \beta}{\sin \gamma} \right) \right\} \right]_0^\gamma = -\frac{\pi}{8} \sin^3 \gamma \end{aligned}$$

$$\begin{aligned} 4(a) \quad & \cos^2 \beta \frac{\sin^2 \beta}{\sin \gamma} \, d(\sin \alpha) \, d\beta \\ & = \frac{1}{2 \sin \gamma} \left[\beta - \frac{1}{2} \left(\beta + \frac{\sin 4\beta}{4} \right) \right]_0^\gamma \\ & = \frac{1}{4 \sin \gamma} \left[\gamma - \sin \gamma \cos \gamma (\cos^2 \gamma - \sin^2 \gamma) \right] \end{aligned}$$

for this case, $\beta_N = 0$, $\theta_S = \pi/2$

$$\frac{I_2}{\Delta A_2} = \frac{a_e I_S}{4 \pi} \left[\frac{1}{\sin \gamma} \left\{ \gamma - \sin \gamma \cos^3 \gamma + \cos \gamma \sin^3 \gamma \right\} - \frac{\pi}{2} \sin^3 \gamma \right]$$



CASE III

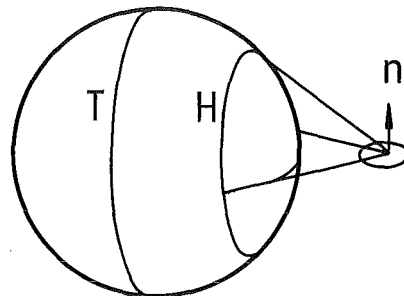
$\theta_S = 0$, $\beta_N = \pi/2$. Integrands 5, 6, 9, 10 remain.

$$5. \quad \cos \alpha_N \sin^2 \beta \cos \beta \cos \psi \cos a$$

$$6. \quad \sin \alpha_N \sin^2 \beta \cos \beta \cos \psi \sin a$$

$$7. \quad \cos \alpha_N \sin^3 \beta \quad \sin \psi \cos a$$

$$8. \quad \sin \alpha_N \sin^3 \beta \quad \sin \psi \sin a$$



which combine as

$$(5, 6)(a) \quad \sin^2 \beta \frac{\cos \beta}{\sin \gamma} \sqrt{\sin^2 \gamma - \sin^2 \beta} \cos(a - \alpha_N)$$

$$(7, 8)(a) \quad \frac{\sin^4 \beta}{\sin \gamma} \cos(a - \alpha_N)$$

and $(a - \alpha_N)$ ranges $(-\pi/2, +\pi/2)$ integrating to a factor 2.

Then with respect to β the integration gives, similar to case II,
 $(5, 6)(b) + \frac{\pi}{8} \sin^3 \gamma$

$$\text{and } \frac{1}{\sin \gamma} \left[\frac{3}{8} \gamma - \frac{1}{2} \sin \gamma \cos \gamma + (\sin \gamma \cos^2 \gamma - \cos \gamma \sin^2 \gamma) \right]$$

so

$$\frac{I_2}{\Delta A_2} = \frac{a_e I_S}{8} \left[\sin^3 \gamma + \frac{1}{\pi \sin \gamma} (3\gamma - 4 \sin \gamma \cos \gamma + \sin \gamma \cos^2 \gamma - \cos \gamma \sin^2 \gamma) \right]$$

CASE IV

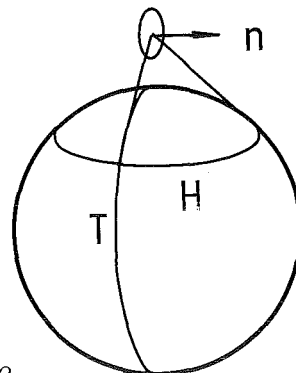
$\theta_S = \pi/2$, $\beta_N = \pi/2$, $\alpha_N = 0$.
 Integrands 7 and 11 remain with
 a ranging $-\pi/2, +\pi/2$

$$(7) \quad -\sin^3 \beta \cos \psi \cos^2 a \, da \, d\beta$$

$$(11) \quad \sin^2 \beta \cos \beta \sin \psi \cos^2 a \, da \, d\beta$$

becoming, through a ,

$$- \frac{\pi}{2} \left(\sin^3 \beta \sqrt{1 - \frac{\sin^2 \beta}{\sin^2 \gamma}} - \frac{\sin^3 \beta}{\sin \gamma} \cos \beta \right) d\beta$$



and, through β ,

$$\begin{aligned} & \frac{\pi}{2 \sin \gamma} \left\{ \frac{1}{2} \left[-\sin \gamma - \cos^2 \gamma \ln \left(\frac{\cos \gamma}{1 + \sin \gamma} \right) \right] \right. \\ & \quad \left. + \frac{1}{4} \left[-\sin^3 \gamma - \frac{\cos^2 \gamma \sin \gamma}{2} - \frac{\cos^4 \gamma}{2} \ln \left(\frac{\cos \gamma}{1 + \sin \gamma} \right) + \sin^4 \gamma \right] \right\} \end{aligned}$$

which is $\frac{I_2}{\Delta A_2} / \frac{I_S a_e}{\pi}$

CASE V

$\theta_S = \pi/2$, $\beta_N = \pi/2$, $\alpha_N = \pi/2$. α ranges $(0, \pi/2)$ giving $\pi/4$ in α . Integrands 8 and 12 survive.

$$(8) \quad -\sin^3 \beta \sqrt{1 - \frac{\sin^2 \beta}{\sin^2 \gamma}} \sin \alpha \, d\alpha \, d\beta$$

$$(12) \quad \sin^2 \beta \cos \beta \sin \psi \sin \alpha \cos \alpha \, d\alpha \, d\beta$$

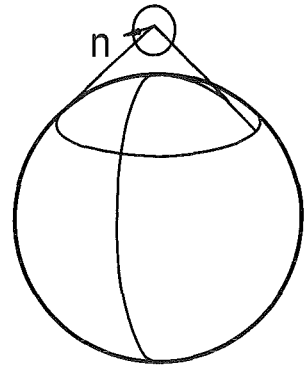
(12) goes simply to

$$(12)(a) \quad + \frac{\sin^4 \gamma}{8}$$

(8) gives

$$(8)(a) \quad \frac{1}{2 \sin \gamma} \left[-\sin \gamma \left(\frac{3}{2} + \frac{\cos^2 \gamma}{4} \right) + \cos^2 \gamma \left(1 + \frac{\cos^2 \gamma}{4} \right) \ln \left(\frac{1 + \sin \gamma}{\cos \gamma} \right) \right]$$

so $[12(a) + 8(a)]$ gives $\frac{I_2}{\Delta A_2} / \frac{I_S a_e}{\pi}$



APPENDIX III

EARTH RADIANCE INTEGRAL

We must evaluate

$$I = \frac{1}{\pi} \int_{\beta_{\min}}^{\beta_{\max}} \int_{\Delta a_{\min}}^{\Delta a_{\max}} \cos \xi (a, \beta, a_N, \beta_N) \sin \beta \, d\beta \, d\Delta a \quad (1)$$

For all $[a, \beta]$ for which, with $\Delta a = a - a_N$,

$$\cos \xi = \cos \beta \cos \beta_N + \sin \beta \sin \beta_N \cos \Delta a \geq 0 \quad (2)$$

Integrating with respect to Δa

$$I = \frac{1}{\pi} \int_{\beta_{\min}}^{\beta_{\max}} \left[\cos \beta_N \cos \beta \sin \beta \Delta a + \sin \beta_N \sin^2 \beta \sin \Delta a \right]_{\Delta a_{\min}}^{\Delta a_{\max}} d\beta \quad (3)$$

By symmetry and oddness of Δa , $\sin \Delta a$ (both zero at $\Delta a = 0$)

$$I = \frac{2}{\pi} \int_{\beta_{\min}}^{\beta_{\max}} \left[\cos \beta_N \cos \beta \sin \beta \Delta a_{\max} + \sin \beta_N \sin^2 \beta \sin \Delta a_{\max} \right] d\beta \quad (4)$$

Whenever $\xi = \pi/2$ is a boundary curve for the integral the relation between β and $\Delta a_{\max}(\beta, \beta_N)$ is obtained from (2) set equal zero, giving

$$\cos \Delta a_{\max}(\beta, \beta_N) = -\cot \beta_N \cot \beta \quad (5)$$

Finally we obtain, when $\xi = \pi/2$ is a boundary,

$$I_{\xi} = \frac{2}{\pi} \int_{\beta_{\min}}^{\beta_{\max}} \left[\cos \beta_N \cos \beta \sin \beta \cos^{-1}(-\cot \beta_N \cot \beta) + \sin \beta_N \sin^2 \beta \sqrt{1 - \cot^2 \beta_N \cot^2 \beta} \right] d\beta \quad (6)$$

While, when Δa may run its full range $[0, \pi]$ ($\sin \Delta a = 0$),

$$I_{\pi} = 2 \int_{\beta_{\min}}^{\beta_{\max}} \cos \beta_N \cos \beta \sin \beta \, d\beta = \cos \beta_N \sin^2 \beta \Big|_{\beta_{\min}}^{\beta_{\max}} \quad (7)$$

To integrate (6) we first simplify: Let $A = \sin \beta_N$, $B = \cos \beta_N$

$$I_{\xi} = \frac{1}{\pi} \int_{\beta_{\min}}^{\beta_{\max}} B \cos^{-1} \left(-\frac{B}{A} \cot \beta \right) d(\sin^2 \beta) - \frac{2}{\pi} \int_{\beta_{\min}}^{\beta_{\max}} \sqrt{A^2 - \cos^2 \beta} \, d(\cos \beta) \quad (8)$$

Integrating by parts the first part of (8)

$$I_{\xi} = \frac{1}{\pi} \left[B \cos^{-1} \left(-\frac{B}{A} \cot \beta \right) \sin^2 \beta \right]_{\beta_{\min}}^{\beta_{\max}} - \frac{1}{\pi} \int B \sin^2 \beta \, d \left(\cos^{-1} \left[-\frac{B}{A} \cot \beta \right] \right) - \frac{2}{\pi} \int \sqrt{A^2 - \cos^2 \beta} \, d(\cos \beta) \quad (9)$$

which reduces to

$$I_{\xi} = \frac{1}{\pi} \left[B \cos^{-1} \left(-\frac{B}{A} \cot \beta \right) \sin^2 \beta \right] - \frac{1}{\pi} \int \frac{B^2 \, d(\cos \beta)}{\sqrt{A^2 - \cos^2 \beta}} - \frac{2}{\pi} \int \sqrt{A^2 - \cos^2 \beta} \, d(\cos \beta) \quad (10)$$

The last two integrals are standard forms giving

$$I_{\xi} = \frac{1}{\pi} \left[B \cos^{-1} \left(-\frac{B}{A} \cot \beta \right) \sin^2 \beta \right]_{\beta_{\min}}^{\beta_{\max}} - \frac{B^2}{\pi} \sin^{-1} \left(\frac{\cos \beta}{A} \right) \Big|_{\beta_{\min}}^{\beta_{\max}} - \frac{1}{\pi} \left(\cos \beta \sqrt{A^2 - \cos^2 \beta} + A^2 \sin^{-1} \left(\frac{\cos \beta}{A} \right) \right) \Big|_{\beta_{\min}}^{\beta_{\max}}$$

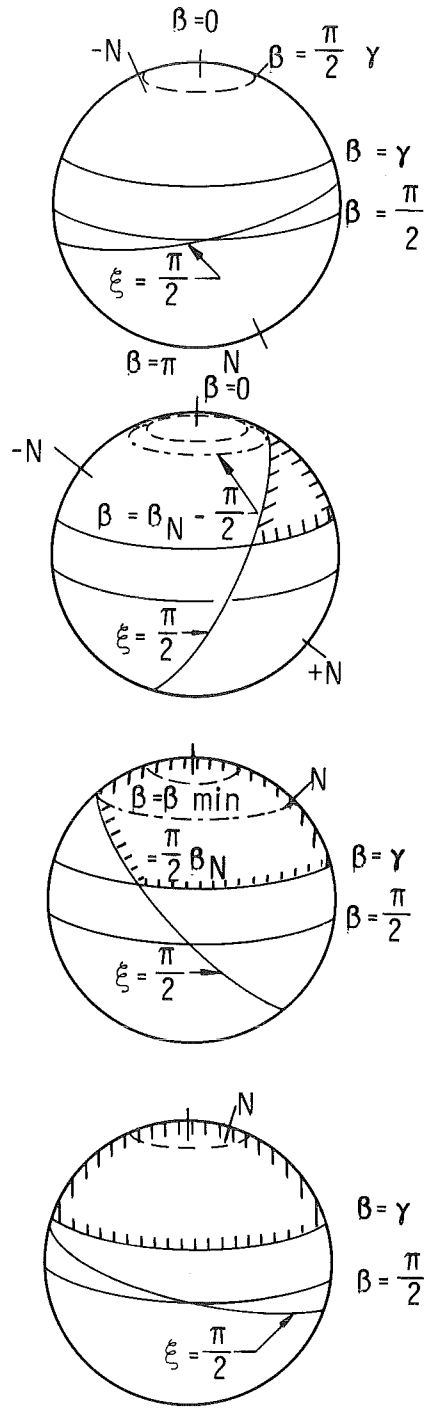
By definition (prior to (8)) $A^2 + B^2 = 1$, hence

$$I_{\xi} = \frac{1}{\pi} \left[B \cos^{-1} \left(-\frac{B}{A} \cot \beta \right) \sin^2 \beta \right] - \frac{1}{\pi} \sin^{-1} \frac{\cos \beta}{A} \Big|_{\beta_{\min}}^{\beta_{\max}} - \frac{1}{\pi} \cos \beta \sqrt{A^2 - \cos^2 \beta} \Big|_{\beta_{\min}}^{\beta_{\max}} \quad (11)$$

and this is defined only for $\pi/2 - \gamma \leq \beta_N \leq \pi/2 + \gamma$, $\beta < \pi/2 - \beta_N$. From (11) and (7), all cases are derived. The integrations are abbreviated here. (See Figs. III-1 and III-2.)

Case 1. I_{π} is the type: $I_1 \equiv 0$

$$\text{Case 2. } I_2 = \frac{2}{\pi} \int_{\beta_{\min} = \beta_N - \pi/2}^{\gamma} \Delta \alpha(\beta, \beta_N) \, d\beta \quad \cdot \quad I_{\xi} \text{ is the type.}$$



Case 1. $\beta_N \geq \frac{\pi}{2} + \gamma$

None of Horizon Circle in View from N.

$$I_1 = 0 \text{ for } \pi \geq \beta_N \geq \frac{\pi}{2} + \gamma$$

Case 1, 2 $I_{1,2} = 0$ $\beta_N = \frac{\pi}{2} + \gamma$

Case 2. N in Hemisphere of $\beta = \pi$

$$\frac{\pi}{2} \leq \beta_N \leq \frac{\pi}{2} + \gamma$$

$$I_2 = \frac{1}{\pi} \cos \beta_N \sin^2 \gamma \left(\sin^{-1} \sqrt{\frac{\sin^2 \beta_N - \cos^2 \gamma}{\sin \beta_N \cos \gamma}} \right)$$

$$- \frac{1}{\pi} \left(\sin^{-1} \frac{\cos \gamma}{\sin \beta_N} + \cos \gamma \sqrt{\sin^2 \beta_N - \cos^2 \gamma} \right) + \frac{1}{2}$$

Case 2, 3 $\beta_N = \frac{\pi}{2}$

$$I_{2,3} = \frac{1}{\pi} \left(\gamma - \sin \gamma \cos \gamma \right)$$

Case 3. N in Hemisphere of $\beta = 0$

$$\frac{\pi}{2} - \gamma \leq \beta_N \leq \frac{\pi}{2}$$

$$I_3 = \frac{1}{\pi} \cos \beta_N \sin^2 \gamma \left(\pi - \sin^{-1} \sqrt{\frac{\sin^2 \beta_N - \cos^2 \gamma}{\sin \beta_N \cos \gamma}} \right)$$

$$- \frac{1}{\pi} \left(\sin^{-1} \frac{\cos \gamma}{\sin \beta_N} + \cos \gamma \sqrt{\sin^2 \beta_N - \cos^2 \gamma} \right) + \frac{1}{2}$$

Case 3, 4 $\beta_N = \frac{\pi}{2} - \gamma$

$$I_{3,4} = \sin^3 \gamma$$

Case 4. All Horizon Circle in View from N.

$$0 \leq \beta_N \leq \frac{\pi}{2} - \gamma$$

$$I_4 = \cos \beta_N \sin^2 \gamma$$

Case 5. $\beta_N = 0$

$$I_5 = \sin^2 \gamma$$

Fig. III-1 Cases of the Earth Radiance Integral

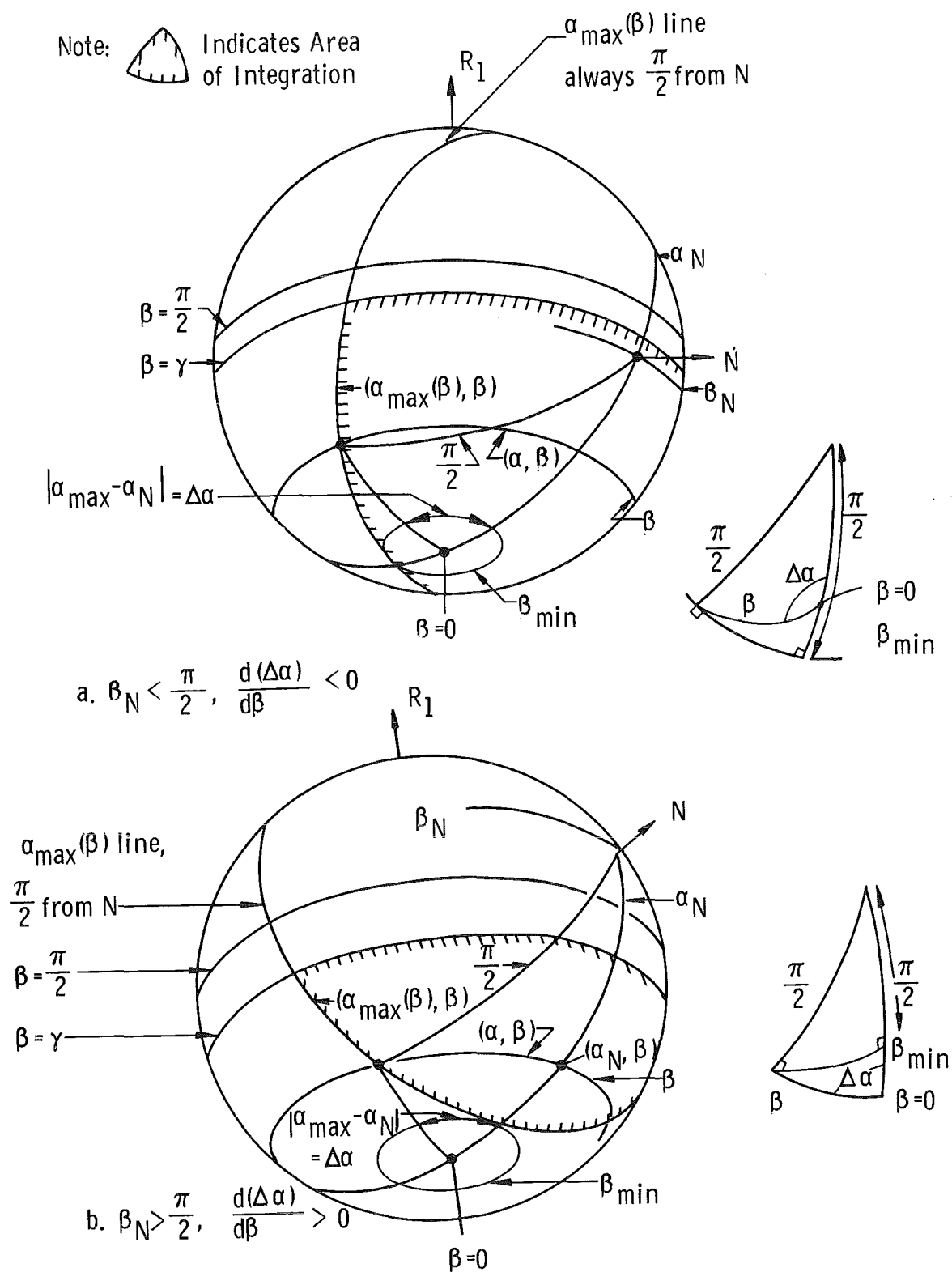


Fig. III-2 Horizon and Normal Limits on (α, β)

APPENDIX IV

SAMPLE PROFILE

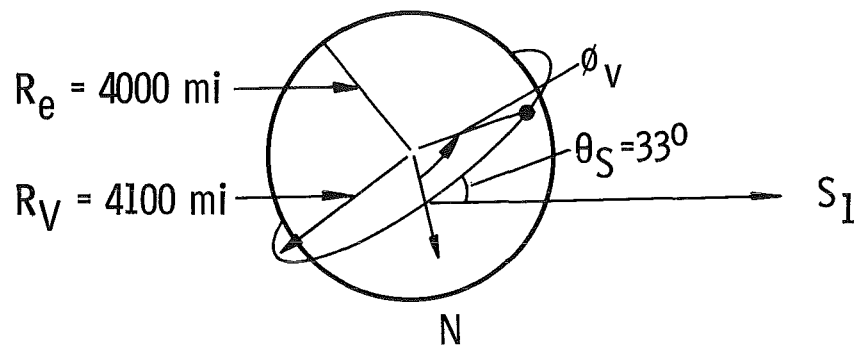
To illustrate the nature of the albedo-earth radiance profiles, we take as model a cone-cylinder vehicle, in a circular orbit, tangent oriented. The cone half-angle is taken to be 27 deg, and the orbit altitude is 100 miles above the earth surface, assumed 4000-mile radius. The orbit is inclined 33 deg to the sun direction (Fig. IV-1).

We plot the earth radiance profile integrals in Fig. IV-2 for cone and cylinder. These are constant functions, independent of time, for the orbit model chosen.

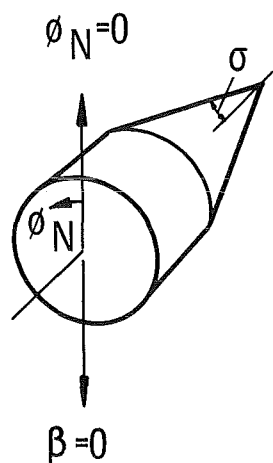
In Fig. IV-3, the cylinder albedo profiles are shown for $\phi_V = 0$, 90 deg. By symmetry, these functions repeat in reverse from 90 to 180 deg. Note that the function tails vanish at about $\pm (\pi/2 - \gamma)$ of $\phi_N = 0$ ($\beta_N = \pi$); further the functions become everywhere zero for about $\pm \gamma$ of $\phi_V = 270$ deg, i. e. while eclipse occurs.

In Figs. IV-4, IV-5, the cone albedo profiles are shown for $\phi_V = 0$, 180 deg. Because the receiving surface is a cone, symmetry fails, and even the top of the cone receives illumination (the tails do not vanish).

These functions were obtained by numerical integration as mentioned in section 4.3.



a. Orbit Model



Dimensions of Apollo-type Vehicle (Fig. 3)

b. Vehicle Model

Fig. IV-1

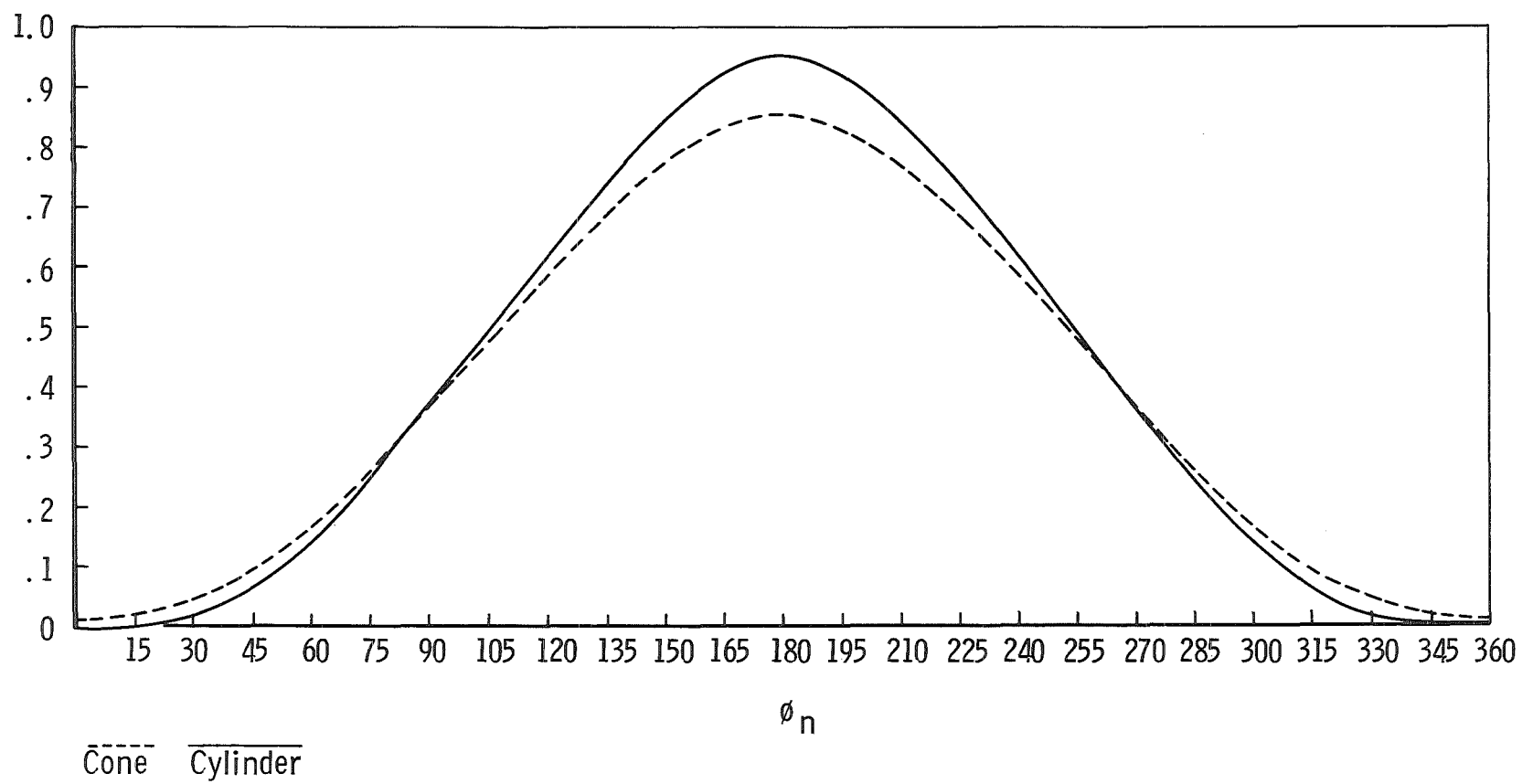


Fig. IV-2 Earth Radiance Profiles

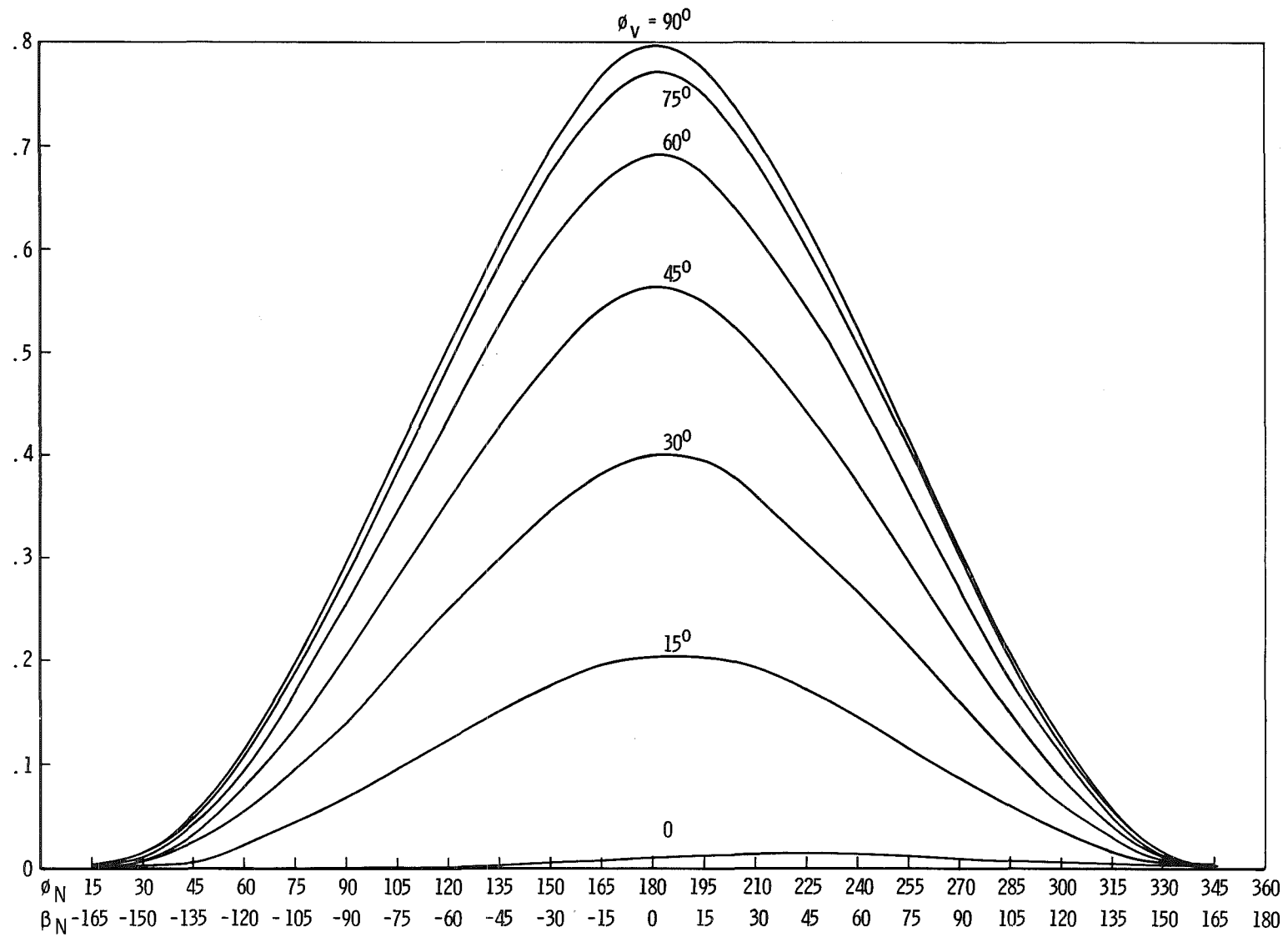


Fig. IV-3 Albedo - Cylinder Profiles

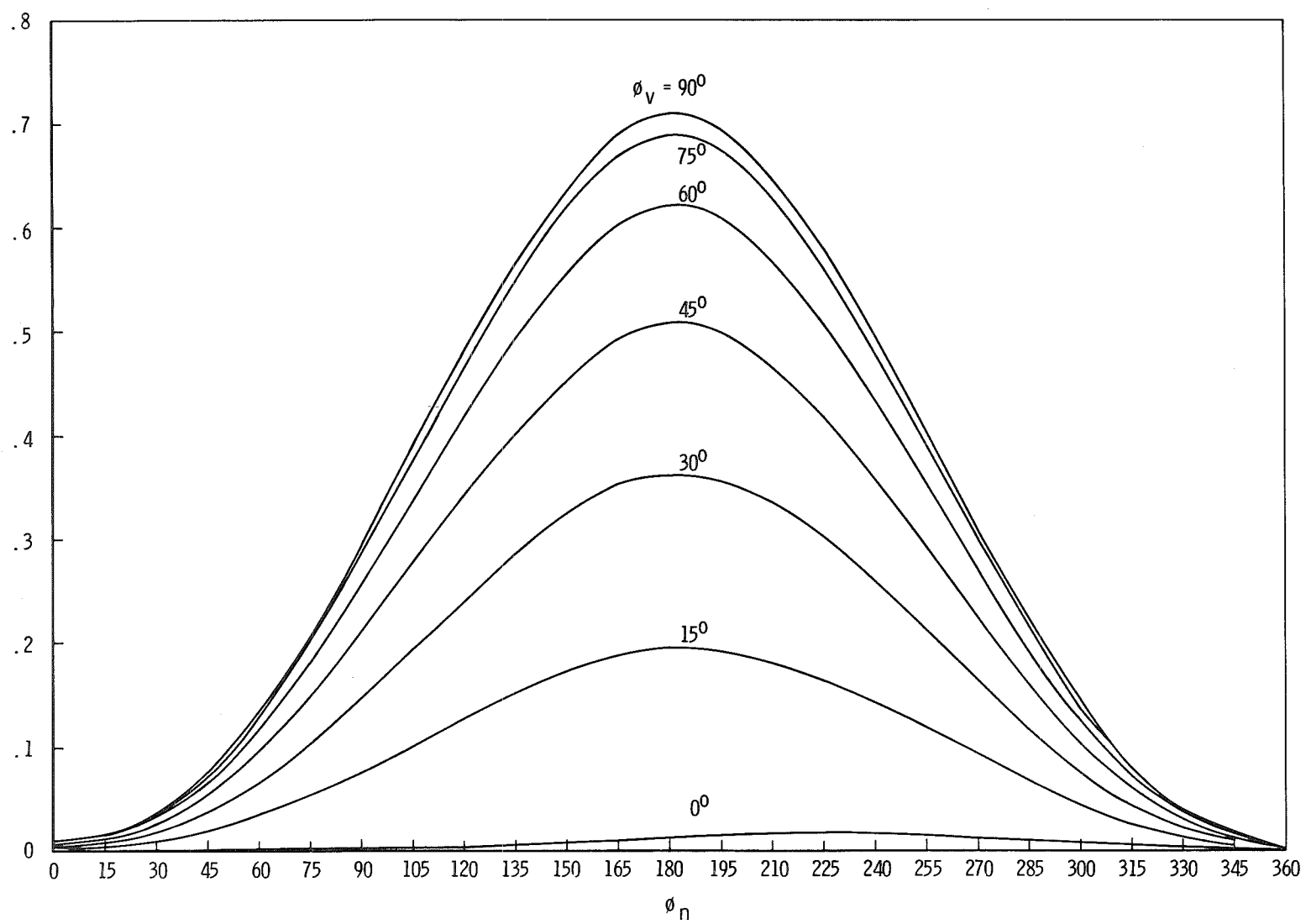


Fig. IV-4 Albedo Cone Profiles

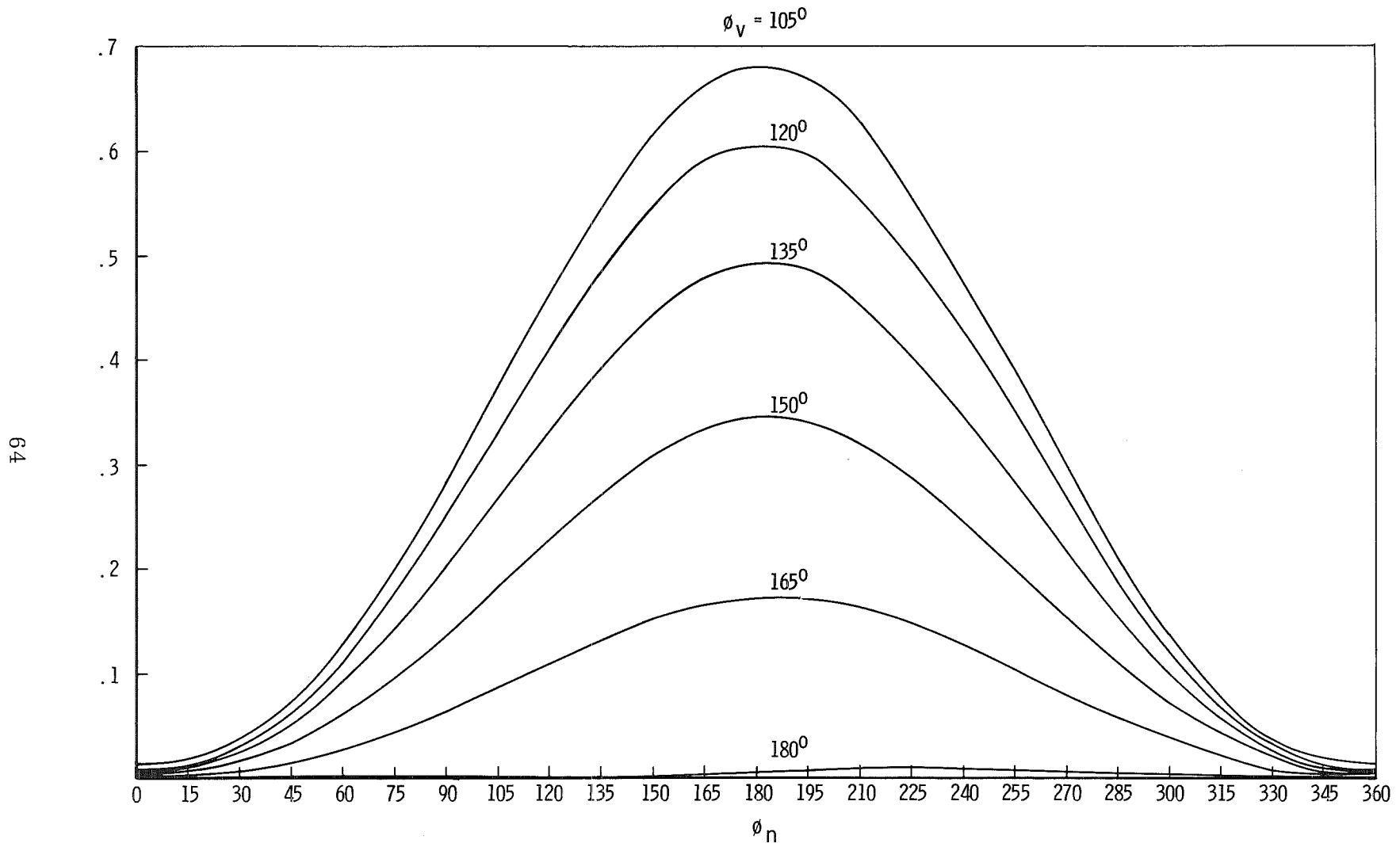


Fig. IV-5 Albedo Cone Profiles